

Thermodynamic Limit in Learning Period Three

Yuichiro Terasaki^{1,*} and Kohei Nakajima^{2,3,†}

¹*Department of Mechano-Informatics, The University of Tokyo, Tokyo 113-8656, Japan*

²*Graduate School of Information Science and Technology,
The University of Tokyo, Tokyo 113-8656, Japan*

³*Next Generation Artificial Intelligence Research Center,
The University of Tokyo, Tokyo 113-8656, Japan*

(Dated: September 13, 2024)

A continuous one-dimensional map with period three includes all periods. This raises the following question: Can we obtain any types of periodic orbits solely by learning three data points? In this letter, we report the answer to be yes. Considering a random neural network in its thermodynamic limit, we show that under certain conditions, learning period three can embed attractors with all periods into the network as a bifurcation after learning. The associated universality is explained by a topological conjugacy between the trained network and the classical logistic map.

With the advent of reservoir computing (RC) [1], which exploits the dynamics of high-dimensional dynamical systems for learning, many interesting properties of random networks have been discovered from a dynamical systems perspective. For example, with a fixed-weight random recurrent neural network, the so-called echo-state network (ESN) [2]—as a reservoir—we can create an autonomous system that emulates target chaotic systems by simply fitting its readout layer [3, 4]. Such an attractor-embedding ability is linked to the existence of the generalized synchronization between an input dynamical system and a reservoir [4–7]. In addition, recent studies have revealed that RC can simultaneously embed multiple attractors [8] and may have untrained attractors that are not part of the training data [8–15]. Surprisingly, a successful reservoir computer only needs a few pairs of bifurcation parameter values and corresponding trajectories to reconstruct the entire bifurcation structure of a target system [10–14]. These properties are valuable, for example, in the context of robot locomotion control using dynamical system attractors that can significantly reduce the training data [16–18]. Thus, the powerful generalization and multifunctionality aspects of RC are related to the dynamical systems properties of a learning machine.

In one-dimensional discrete dynamical systems, there are two significant theorems on periodic orbits [19–21]:

Theorem 1 (Sharkovsky) *If a continuous map $f : I \rightarrow I$ has a periodic point of period m and $m \succ n$, then f also has a periodic point of period n .*

Theorem 2 (Li–Yorke) *If a continuous map $f : I \rightarrow I$ has a point $a \in I$ for which the points $b = f(a)$, $c = f(f(a))$, and $d = f(f(f(a)))$ satisfy*

$$d \leq a < b < c \quad (\text{or} \quad d \geq a > b > c),$$

then f has a periodic point of period k for every $k \in \mathbb{N}$.

Note that the interval I does not need to be closed or bounded. Here, the ordering of positive integers \succ in

Theorem 1 is called the Sharkovsky ordering and is given below:

$$\begin{aligned} 3 \succ 5 \succ 7 \succ 9 \succ \dots \succ 2 \cdot 3 \succ 2 \cdot 5 \succ 2 \cdot 7 \succ \dots \\ \succ 2^2 \cdot 3 \succ 2^2 \cdot 5 \succ 2^2 \cdot 7 \succ \dots \succ 2^3 \succ 2^2 \succ 2 \succ 1. \end{aligned} \quad (1)$$

We write $m \succ n$ whenever m is to the left of n in Eq. (1). As a consequence of both theorems, a continuous one-dimensional map with period three has all periods.

Now, the following natural question arises: Can we obtain all the periods in the network through training only period three? If we successfully train period three in one-dimensional dynamics, then the straightforward answer is “yes.” However, this question is somewhat naive, since the above theorems do not reveal whether the obtained periods are stable. Instead, we should ask the following question: Which kind of stable orbits (attractors) can we obtain by learning period three (LP3)? This paper is devoted to theoretically answer this question in terms of all aspects.

To clarify what LP3 implies, we need to create an one-dimensional recurrent neural network with target period three. LP3 with ESN, as in the standard RC scheme, will violate the assumption of the above two theorems due to the high-dimensionality of the resulting dynamics. Thus, here, we consider training the readout weights of a two-layer random feedforward neural network to learn period three [22–25]: $f_N(x) \equiv \frac{1}{\sqrt{N}} \sum_{i=1}^N W_i^{\text{out}} \phi(h_i(x))$, $h_i(x) \equiv W_i^{\text{in}} x + b_i^{\text{in}}$, where $x \in \mathbb{R}$ is an input of the network; $W^{\text{in}} \in \mathbb{R}^{N \times 1}$ and $b^{\text{in}} \in \mathbb{R}^N$ are the input weights and biases, respectively, randomly drawn from a Gaussian distribution with zero mean and variance given by σ^2 ; $\phi: \mathbb{R} \rightarrow \mathbb{R}$ is an activation function; and $W^{\text{out}} \in \mathbb{R}^{1 \times N}$ is the output weights matrix optimized by a learning method described subsequently (see Sec. IA and Sec. ID in the Supplementary Material (SM) [26] for networks with output bias and uniform distribution). Actually, this model can be regarded as a special case of an ESN in the limit where the spectral radius of the adjacency matrix goes to zero. In addition, we denote the trained

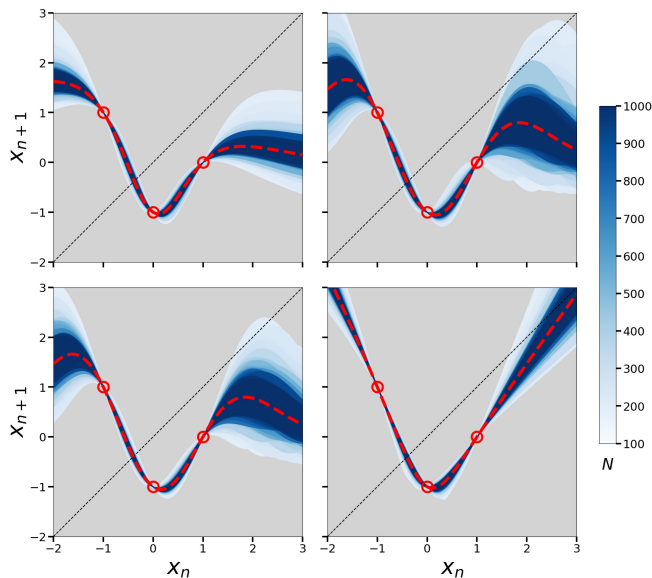


FIG. 1. Trained maps f_N^* for activation functions $\phi = \text{erf}$ (top left), \sin (top right), \cos (bottom left), and ReLU (bottom right), with target period three $\mathcal{D} = \{-1, 1, 0\}$ and scale of weights $\sigma = 1.0$. The blue-colored areas indicate the maximum–minimum regions of f_N^* for 100 different realizations. The red circles and the red dotted lines show \mathcal{D} and the thermodynamic limit f_∞^* , respectively. The darkness of blue corresponds to the number of nodes N , describing that f_N^* degenerates into f_∞^* as N increases.

network output by $f_N^*(x)$ and call σ the scale of weights. With the trained network f_N^* , we study the dynamical system $x_{n+1} = f_N^*(x_n)$ created from a closed loop that connects its input and output. The attractors of f_N^* should depend on the network structure, including the realizations of W^{in} and b^{in} and the choice of ϕ , which makes the above question non-trivial. Hereafter, we consider the following specific activation functions: bounded and smooth $\phi = \text{erf}, \sin, \cos$, and unbounded and non-smooth $\phi = \text{ReLU}$.

Our findings are threefold. First, concerning general training data, we show that the trained map f_N^* degenerates into its thermodynamic limit f_∞^* as N increases (Fig. 1) under certain assumptions. Second, in LP3, we reveal that almost all acquired periods are unstable; it has characteristic attractors corresponding to the choice of target period three, nonlinearity ϕ , and scale of weights σ . Third, we prove that neural networks with certain activations can externalize all the latently acquired unstable periods through LP3 as attractors after learning, as a universal bifurcation with regard to the feedback strength. We discuss the range of applicability of our proposed approach to physical learning machines at the end of this paper.

We denote the training dataset and its number by $\mathcal{D} \subseteq \mathbb{R} \times \mathbb{R}$ and $|\mathcal{D}|$, respectively, and assume $N \geq |\mathcal{D}|$. We use \mathcal{X} and \mathcal{Y} vectors to denote the input and out-

put data and define them as $\mathcal{X} \equiv [x_1, \dots, x_{|\mathcal{D}|}]$, $\mathcal{Y} \equiv [y_1, \dots, y_{|\mathcal{D}|}] \in \mathbb{R}^{|\mathcal{D}|}$, where $(x_i, y_i) \in \mathcal{D}$. In LP3 ($a \mapsto b \mapsto c \mapsto a \mapsto \dots$), the target input–output pairs are $\mathcal{D} = \{(a, b), (b, c), (c, a)\}$, $\mathcal{X} = [a, b, c]$, and $\mathcal{Y} = [b, c, a]$. For the sake of simplicity, we write $\mathcal{D} = \{a, b, c\}$ and assume $a < b$. Note that a period-3 orbit is of two types: $\{a, b, c\}$ and $\{b, a, c\}$. Generally, a period- n orbit has $(n-1)!$ types. For a given \mathcal{D} , we optimize W^{out} by least square regression with a minimum norm solution (“extreme learning machine” [23, 24, 27]) or “ridgeless” regression [28–31]:

$$f_N^*(x) = \lim_{\lambda \searrow 0} \hat{\Theta}(x, \mathcal{X}) \left(\hat{\Theta} + \lambda I_{|\mathcal{D}|} \right)^{-1} \mathcal{Y}, \quad (2)$$

where $\hat{\Theta}(x, \mathcal{X}) \in \mathbb{R}^{1 \times |\mathcal{D}|}$ and $\hat{\Theta} \equiv \hat{\Theta}(\mathcal{X}, \mathcal{X}) \in \mathbb{R}^{|\mathcal{D}| \times |\mathcal{D}|}$ are the matrices given in the following manner:

$$\hat{\Theta}(x, \mathcal{X})_i \equiv \hat{\Theta}(x, x_i), \quad \hat{\Theta}_{ij} \equiv \hat{\Theta}(x_i, x_j), \quad (3)$$

$$\hat{\Theta}(x, y) \equiv \mathcal{R}(x)^\top \mathcal{R}(y) = \frac{1}{N} \sum_{i=1}^N \phi(h_i(x)) \phi(h_i(y)), \quad (4)$$

$$\mathcal{R}(x)_i \equiv \frac{1}{\sqrt{N}} \phi(h_i(x)), \quad \mathcal{R}(x) \in \mathbb{R}^N. \quad (5)$$

We note that Eq. (2) is equivalent to fit W^{out} with the pseudoinverse of the matrix of hidden states $\mathcal{R}(\mathcal{X}) \equiv [\mathcal{R}(x_1) \cdots \mathcal{R}(x_{|\mathcal{D}|})] \in \mathbb{R}^{N \times |\mathcal{D}|}$ [27]: $(W^{\text{out}})^* = \mathcal{Y}^\top \mathcal{R}(\mathcal{X})^+$. If the matrix $\hat{\Theta}$ has full rank, Eq. (2) has the following closed-form expression:

$$f_N^*(x) = \hat{\Theta}(x, \mathcal{X}) \hat{\Theta}^{-1} \mathcal{Y}. \quad (6)$$

By the law of large numbers, $\hat{\Theta}(x, y)$ (Eq. (4)) converges in probability to $\Theta(x, y)$ —that is the expectation over random variables $[\omega, \beta] \sim \mathcal{N}(\mathbf{0}, \sigma^2 I)$ —in the limit $N \rightarrow \infty$ because the components of W^{in} and b^{in} follow an iid Gaussian distribution [32]:

$$\Theta(x, y) = \frac{1}{2\pi\sigma^2} \int d\omega d\beta \phi(\omega x + \beta) \phi(\omega y + \beta) e^{-\frac{\omega^2 + \beta^2}{2\sigma^2}}. \quad (7)$$

In our model, $\Theta(x, y)$ coincides with the neural tangent kernel (NTK) and the neural network gaussian process (NNGP) kernel [32, 33]. Defining $\Theta(x, \mathcal{X})$ and Θ in the same manner as $\hat{\Theta}(x, y)$, we acquire $f_\infty^*(x)$, since $f_N^*(x)$ (Eq. (6)) is calculated from only the values of $\hat{\Theta}(x, y)$:

$$f_\infty^*(x) = \Theta(x, \mathcal{X}) \Theta^{-1} \mathcal{Y}, \quad (8)$$

where we again assume Θ to have full rank. This assumption is valid if ϕ is a non-polynomial continuous function and \mathcal{X} consists of $|\mathcal{D}|$ distinct points, according to Theorem 3 in Ref. [34] (Sec. 1B in the SM [26], which includes Ref. [35]). In addition, the output of the infinite-width ESN also reduces to a form similar to that of Eq. (8) with time-varying recurrent kernels [36–38].

With regard to LP3, f_∞^* is given by

$$f_\infty^*(x) = \begin{bmatrix} \Theta(x, a) \\ \Theta(x, b) \\ \Theta(x, c) \end{bmatrix}^\top \begin{bmatrix} \Theta(a, a) & \Theta(a, b) & \Theta(a, c) \\ \Theta(b, a) & \Theta(b, b) & \Theta(b, c) \\ \Theta(c, a) & \Theta(c, b) & \Theta(c, c) \end{bmatrix}^{-1} \begin{bmatrix} b \\ c \\ a \end{bmatrix}. \quad (9)$$

To investigate the dynamics of f_∞^* , we compute the trajectory $\{x_n\}_{n=0}^T$ of $T + 1 \gg 1$ steps with an initial state x_0 and calculate the Lyapunov exponent and period of attractors from the trajectories. The Lyapunov exponent expresses the sensitivity of a dynamical system to initial conditions and is calculated using the following equation:

$$\lambda_T = \frac{1}{T} \sum_{n=1}^T \ln \left| \frac{df_\infty^*}{dx}(x_n) \right|. \quad (10)$$

We regard a trajectory of f_∞^* as chaotic when $\lambda_T > 0$. Note that the derivative of f_∞^* is calculated by

$$\frac{df_\infty^*}{dx}(x) = \frac{\partial \Theta}{\partial x}(x, \mathcal{X}) \Theta^{-1} \mathcal{Y}. \quad (11)$$

We also calculate the period of attractors as the minimum integer $n \in [1, n_{\max}]$ that satisfies the following inequality ($n_{\max} = 10$ or 20 and $\varepsilon = 10^{-12}$ except as otherwise noted):

$$\frac{|(f_\infty^*)^n(x_T) - x_T|}{\max\{|x_T|, |(f_\infty^*)^n(x_T)|\}} \leq \varepsilon, \quad (12)$$

$$\text{where } (f_\infty^*)^1 \equiv f_\infty^*, (f_\infty^*)^{k+1} \equiv f_\infty^* \circ (f_\infty^*)^k.$$

For $\phi = \text{erf}, \sin, \cos, \text{ReLU}$, there exist the analytic solutions of $\Theta(x, y)$. Following Williams [39], the NTK for $\phi = \text{erf}$ is expressed as follows (see Sec. IC in the SM [26] regarding the NTKs for $\phi = \sin, \cos, \text{ReLU}$, which includes Ref. [40]):

$$\Theta^{\text{erf}}(x, y) = \frac{2}{\pi} \arcsin \frac{2\sigma^2(1 + xy)}{\sqrt{[1 + 2\sigma^2(1 + x^2)][1 + 2\sigma^2(1 + y^2)]}}. \quad (13)$$

We note that the trajectories for a bounded activation function—such as $\phi = \text{erf}, \sin, \cos$ —are also bounded since $\Theta(x, y)$ (Eq. (7)) is the expectation of the product of ϕ . Moreover, as $\phi = \text{erf}, \sin, \cos$ and their corresponding NTKs are analytic, f_N^* and f_∞^* have finitely many attractors, according to Theorem B in Ref. [41] (Sec. II in the SM [26], which includes Ref. [42]). In contrast, certain trajectories for $\phi = \text{ReLU}$, whose NTK is unbounded, will head toward infinity.

Figure 2 depicts how f_∞^* for $\phi = \text{erf}$ changes as c varies. Note that as long as $\hat{\Theta}$ and Θ have full rank, trained networks completely learn the target orbit \mathcal{D} since $f_N^*(\mathcal{X}) = f_\infty^*(\mathcal{X}) = \mathcal{Y}$. In the case of \mathcal{D} becoming the attractor ($-3 \leq c < -2.2$ and $0 < c \leq 0.22$), which corresponds to the successful attractor embedding

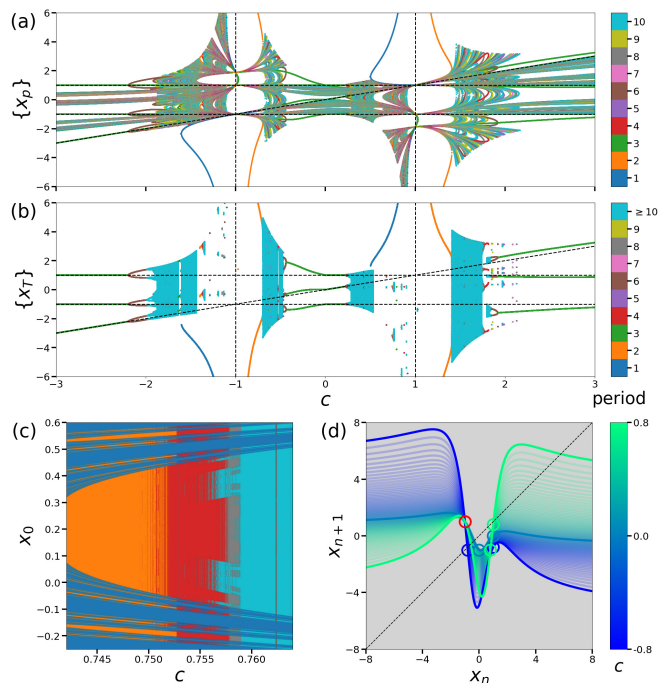


FIG. 2. Change in dynamical system f_∞^* for $\phi = \text{erf}$ with respect to c , with $a = -1$, $b = 1$, and $\sigma = 1.0$. The trajectory $\{x_n\}_{n=0}^T$ of $T = 10^5$ steps is computed with different x_0 and c in given intervals, excluding $c = a, b$. (a) Changes in the acquired periods $\{x_p\}$ of period p , calculated by solving $(f_\infty^*)^p(x_p) = x_p$ (see Sec. V in the SM [26] for details). (b) Bifurcation diagram of the characteristic attractors calculated with $-10 \leq x_0 \leq 10$. The dotted lines indicate \mathcal{D} ; the diagonal lines correspond to varying c . (c) Change in the basin of attraction where f_∞^* has multiple untrained attractors. (d) Change in the map f_∞^* in $-0.8 \leq c \leq 0.8$. The circles indicate \mathcal{D} and the red circle indicates a c -independent point $(a, b) = (-1, 1)$. As c approaches a or b , the folding of f_∞^* around \mathcal{D} becomes larger, making the characteristic attractors wider.

by a learning machine, we observe that f_∞^* has no untrained attractors. However, varying c causes the bifurcation of the embeddable attractors of f_∞^* , resulting in the emergence of untrained attractors: untrained period-3 ($-0.43 \leq c < 0$ and $2 \leq c \leq 3$), chaotic ($c = -0.5, 0.3$, etc.), and multiple attractors ($0.742 \leq c \leq 0.764$, etc.). Consequently, only a handful of attractors appear at a time, and almost all periods latently exist as unstable periods (Fig. 2(a),(b)). Such bifurcation of the characteristic attractors strongly depends on the network settings (see Sec. IV in the SM [26] for the bifurcation diagrams with respect to c and σ , along with the corresponding λ_T , which includes Refs. [43, 44]). We note that as the NTKs for $\phi = \text{erf}, \sin, \cos, \text{ReLU}$ depend on the scaling and translation of inputs, varying a or b , which we fixed, also yields a different bifurcation. Nevertheless, the bifurcation structure has universal symmetry properties under the swapping of a and b (Sec. III in the SM [26]).

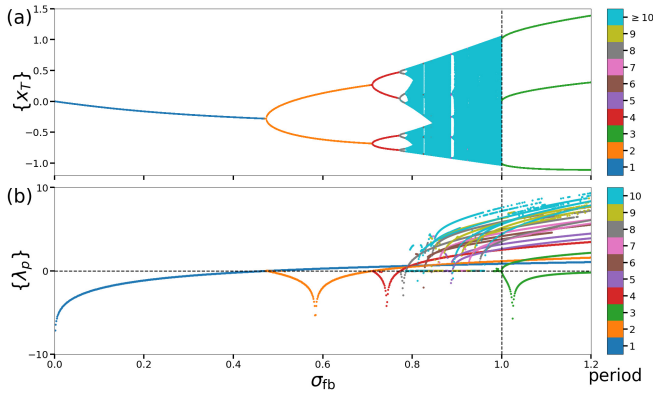


FIG. 3. Change in dynamical system $\sigma_{\text{fb}} f_{\infty}^*$ for $\phi = \text{erf}$ with respect to feedback strength σ_{fb} , with $\mathcal{D} = \{-1, 1, 0\}$ and $\sigma = 1$. (a) Bifurcation diagram calculated with $-10 \leq x_0 \leq 10$ and $T = 10^5$. (b) Stability changes in the acquired periods $\{x_p\}$ of period p , calculated by $\lambda_p \equiv \ln \left| \frac{d}{dx} (\sigma_{\text{fb}} f_{\infty}^*)^p(x_p) \right|$ using the solutions of $(\sigma_{\text{fb}} f_{\infty}^*)^p(x_p) = x_p$. The vertical dotted lines correspond to the network state in LP3 ($\sigma_{\text{fb}} = 1$). The horizontal dotted line indicates the boundary of the stability $\lambda_p = 0$; $\lambda_p < 0$ and $\lambda_p > 0$ mean (locally) stable and unstable, respectively. In this setting, decreasing σ_{fb} toward 0 externalizes the latently existing unstable periods as period-doubling cascades, which is illustrated as the continuous lines of $\{\lambda_p\}$ from $\lambda_p > 0$ (at $\sigma_{\text{fb}} = 1$) to $\lambda_p < 0$ (at some $\sigma_{\text{fb}} \in (0, 1)$).

In particular, if $\Theta(x, y) = \Theta(-x, -y)$, $f_{\infty}^*|_{\mathcal{D}=\{a, -a, c\}}$ is topologically conjugate to $f_{\infty}^*|_{\mathcal{D}=\{-a, a, -c\}}$, and there is a qualitative correspondence between the outside ($c < a, b < c$) and the inside ($a < c < b$) bifurcation structure, if $b \approx -a$ (Fig. 2(a),(b)).

So far, we have only focused on the characteristic attractors of the neural networks in LP3, which are just small parts of latently existing infinitely many periodic orbits. To illuminate the meaning of the latently existing unstable periods, we further extend our learning procedure to varying the readout weights of the trained neural networks [25]. Figure 3 depicts how its attractor changes as the scale of the readout weights—the feedback strength σ_{fb} —varies. We set the network state of LP3 to $\sigma_{\text{fb}} = 1$; this dynamical system is expressed as $\sigma_{\text{fb}} f_{\infty}^*$. Since the network is prohibited from having any periodic orbits except a fixed point $x = 0$ at $\sigma_{\text{fb}} = 0$, all the acquired periods $\{x_p\}$ must disappear at some $\sigma_{\text{fb}} \in (0, 1)$ with $\frac{d}{dx} (\sigma_{\text{fb}} f_{\infty}^*)^p(x_p) = 1$ (tangent bifurcation) due to the differentiability of f_{∞}^* ; some of them may become attractors before dying out. The way of the externalization of latently unstable periods depends on the choice of \mathcal{D} and the network structure (see Fig. S17 in the SM [26]).

Now, let us assume that $\mathcal{D} = \{a, -a, 0\}$ (symmetric LP3) and $\phi = \text{erf}, \sin, \cos$. Surprisingly, this symmetry of \mathcal{D} and differentiability of ϕ will induce further universal bifurcation that externalizes all the latently unstable periods into stable ones after learning, corresponding to the Sharkovsky ordering (Eq. (1)) (see Figs. S18–S20 in the

SM [26] for $\phi = \text{ReLU}$, which induces slightly different externalization). Thanks to the symmetry in the distribution of W^{in} at $W^{\text{in}} = 0$, $\Theta(x, x)$, $\Theta(x, -x)$, and $\Theta(x, 0)$ are even functions of x since $\Theta(x, y) = \Theta(-x, -y)$. Applying $b = -a$ and $c = 0$ to Eq. (9) and exploiting these symmetries, the derivative of f_{∞}^* at $x = 0$ is given as follows:

$$\begin{aligned} \left. \frac{df_{\infty}^*}{dx}(0) \right|_{\mathcal{D}=\{a, -a, 0\}} &= -\frac{a \frac{\partial \Theta}{\partial x}(0, a)}{\Theta(a, a) - \Theta(a, -a)} \\ &= -\frac{\frac{\partial^2 \Theta}{\partial x \partial y}(0, 0) + \mathcal{O}(a)}{2 \frac{\partial^2 \Theta}{\partial x \partial y}(0, 0) + \mathcal{O}(a)} \rightarrow -\frac{1}{2} \quad (a \rightarrow 0). \end{aligned} \quad (14)$$

Note that $\frac{\partial^2 \Theta}{\partial x \partial y}(0, 0) = \mathbb{E}_{\omega, \beta} [\omega^2 \phi'(\beta)^2] > 0$. Next, for $a \ll 1$, the local shape of $f_{\infty}^*(x)$ around $\mathcal{D} = \{a, -a, 0\}$ is well described as a polynomial function $g(x)$. Imposing $g(\mathcal{X}) = \mathcal{Y}$ and $\frac{dg}{dx}(0) = -\frac{1}{2}$, its third-order approximation is uniquely determined as

$$g(x) = a \hat{g}\left(\frac{x}{a}\right), \quad \hat{g}(x) \equiv 1 - \frac{x}{2} - \frac{3x^2}{2} + 0 \cdot x^3, \quad (15)$$

which is topologically conjugate to \hat{g} . Furthermore, under $\mu > 2$ and $\sigma_{\text{fb}} > 0$, $x_{n+1} = \sigma_{\text{fb}} \hat{g}(x_n)$ is topologically conjugate to the logistic map $y_{n+1} = \mu y_n(1 - y_n)$ in the following manner [45]:

$$x_n = -\frac{2}{3} \left[\frac{\mu}{\sigma_{\text{fb}}(\mu)} \left(-y_n + \frac{1}{2} \right) + \frac{1}{4} \right], \quad (16)$$

$$\sigma_{\text{fb}}(\mu) = \frac{4}{5} \sqrt{\frac{\mu}{2} \left(\frac{\mu}{2} - 1 \right) + \frac{1}{100} - \frac{2}{25}}. \quad (17)$$

With $0 < \sigma_{\text{fb}}(\mu_1) \leq \sigma_{\text{fb}}(\mu_2)$ for $2 < \mu_1 \leq \mu_2$ and the Sharkovsky ordering in μ [46, 47], we obtain the Sharkovsky ordering in externalization:

$$\begin{aligned} \sigma_{\text{fb}}[3] &\geq \sigma_{\text{fb}}[5] \geq \dots \geq \sigma_{\text{fb}}[2 \cdot 3] \geq \sigma_{\text{fb}}[2 \cdot 5] \geq \dots \\ &\geq \sigma_{\text{fb}}[2^2 \cdot 3] \geq \dots \geq \sigma_{\text{fb}}[2^2] \geq \sigma_{\text{fb}}[2] \geq \sigma_{\text{fb}}[1], \end{aligned} \quad (18)$$

where we denote by $\sigma_{\text{fb}}[n]$ the least value of σ_{fb} for which $\sigma_{\text{fb}} \hat{g}$ possesses period n as its attractor and $\sigma_{\text{fb}}[1] \equiv 0$. Here, $0 = \sigma_{\text{fb}}[1] \leq \dots \leq \sigma_{\text{fb}}[3] = \sigma_{\text{fb}}(1 + \sqrt{8}) < 1$. Consequently, the universality (Eqs. (15) and (18)) retains no information about network settings N, ϕ, σ or the dataset a , implying the strong convergence of the externalization in symmetric LP3 (see Sec. VI in the SM [26] for a detailed discussion, which includes Ref. [48]). Interestingly, with a small a , we observed the coexistence of the controlled attractors—which come from the universality \hat{g} —and the characteristic attractors—which come from the details of the network structure—in the externalization $\sigma_{\text{fb}} f_{\infty}^*$ (see Fig. S18 in the SM [26]).

Although LP3 is not a necessary condition for achieving period three (learning period two or even random neural networks [49] may have period three, see Fig. S15

and Fig. S21 in the SM [26]), it provides a sufficient condition for embedding attractors with all periods as a universal bifurcation along with externally controllable parameters \mathcal{D} and σ_{fb} —which is our answer to the very first question. LP3 also provides new yet important perspectives in the learning of dynamics. First, even if neural networks completely learn a target orbit \mathcal{D} , they may fail to replicate \mathcal{D} , since its stability depends on the local structure of the trained map f_{∞}^* around \mathcal{D} . Second, LP3 is not a goal, but a groundwork or a primer for updating the connectivity of random networks to generate all types of periodic orbits, including chaos, after learning. Generating network dynamics with a minimal dataset is not just efficient but also compatible with the theoretical analysis, since $f_{\infty}^*(x)$ is described by the multiplication of $\Theta(x, \mathcal{X})$ and Θ^{-1} ; learning dynamics from time series lead to a large $|\mathcal{D}|$ and a nearly singular Θ , making the analysis of f_{∞}^* ineffective.

As an engineering application, we may replace the feedforward network part with a physical system or neuromorphic device [50–52]; embedding desirable dynamics into physical systems would be highly beneficial, for example, in a high-radiation environment in which a computer-simulated attractor may break down [53]. We leave the further analysis on the control of embeddable attractors in physical systems for future work.

We are grateful to Allen Hart for the fruitful discussions on attractor embedding in RC and to the RC seminar members for the stimulating discussions.

* terasaki@isi.imi.i.u-tokyo.ac.jp

† k-nakajima@isi.imi.i.u-tokyo.ac.jp

- [1] K. Nakajima and I. Fischer, *Reservoir Computing* (Springer, Singapore, 2021).
- [2] H. Jaeger, The “echo state” approach to analysing and training recurrent neural networks—with an erratum note, Bonn, Germany: German National Research Center for Information Technology GMD Technical Report **148**, 13 (2001).
- [3] J. Pathak, Z. Lu, B. R. Hunt, M. Girvan, and E. Ott, Using machine learning to replicate chaotic attractors and calculate Lyapunov exponents from data, *Chaos: An Interdisciplinary Journal of Nonlinear Science* **27**, 121102 (2017).
- [4] Z. Lu, B. R. Hunt, and E. Ott, Attractor reconstruction by machine learning, *Chaos: An Interdisciplinary Journal of Nonlinear Science* **28**, 061104 (2018).
- [5] A. Hart, J. Hook, and J. Dawes, Embedding and approximation theorems for echo state networks, *Neural Networks* **128**, 234 (2020).
- [6] L. Grigoryeva, A. Hart, and J.-P. Ortega, Chaos on compact manifolds: Differentiable synchronizations beyond the takens theorem, *Phys. Rev. E* **103**, 062204 (2021).
- [7] L. Grigoryeva, A. Hart, and J.-P. Ortega, Learning strange attractors with reservoir systems, *Nonlinearity* **36**, 4674 (2023).
- [8] A. Flynn, V. A. Tsachouridis, and A. Amann, Multifunctionality in a reservoir computer, *Chaos: An Interdisciplinary Journal of Nonlinear Science* **31**, 013125 (2021).
- [9] A. Flynn, V. A. Tsachouridis, and A. Amann, Seeing double with a multifunctional reservoir computer, *Chaos: An Interdisciplinary Journal of Nonlinear Science* **33**, 113115 (2023).
- [10] L.-W. Kong, H.-W. Fan, C. Grebogi, and Y.-C. Lai, Machine learning prediction of critical transition and system collapse, *Phys. Rev. Res.* **3**, 013090 (2021).
- [11] H. Fan, L.-W. Kong, Y.-C. Lai, and X. Wang, Anticipating synchronization with machine learning, *Phys. Rev. Res.* **3**, 023237 (2021).
- [12] J. Z. Kim, Z. Lu, E. Nozari, G. J. Pappas, and D. S. Bassett, Teaching recurrent neural networks to infer global temporal structure from local examples, *Nature Machine Intelligence* **3**, 316 (2021).
- [13] D. Patel, D. Canaday, M. Girvan, A. Pomerance, and E. Ott, Using machine learning to predict statistical properties of non-stationary dynamical processes: System climate, regime transitions, and the effect of stochasticity, *Chaos: An Interdisciplinary Journal of Nonlinear Science* **31**, 033149 (2021).
- [14] H. Fan, L. Wang, Y. Du, Y. Wang, J. Xiao, and X. Wang, Learning the dynamics of coupled oscillators from transients, *Phys. Rev. Res.* **4**, 013137 (2022).
- [15] A. Röhm, D. J. Gauthier, and I. Fischer, Model-free inference of unseen attractors: Reconstructing phase space features from a single noisy trajectory using reservoir computing, *Chaos: An Interdisciplinary Journal of Nonlinear Science* **31**, 103127 (2021).
- [16] S. Steingrube, M. Timme, F. Wörgötter, and P. Manoonpong, Self-organized adaptation of a simple neural circuit enables complex robot behaviour, *Nature physics* **6**, 224 (2010).
- [17] A. J. Ijspeert, A. Crespi, D. Ryczko, and J.-M. Cabelguen, From swimming to walking with a salamander robot driven by a spinal cord model, *Science* **315**, 1416 (2007).
- [18] N. Akashi, Y. Kuniyoshi, T. Jo, M. Nishida, R. Sakurai, Y. Wakao, and K. Nakajima, Embedding bifurcations into pneumatic artificial muscle, *Advanced Science* **11**, 2304402 (2024).
- [19] K. Burns and B. Hasselblatt, The sharkovsky theorem: A natural direct proof, *The American Mathematical Monthly* **118**, 229 (2011).
- [20] A. M. Blokh and O. M. Sharkovsky, *Sharkovsky Ordering* (Springer, Cham, 2022).
- [21] T.-Y. Li and J. A. Yorke, Period three implies chaos, *The American Mathematical Monthly* **82**, 985 (1975).
- [22] R. Tokunaga, S. Kajiwara, and T. Matsumoto, Reconstructing bifurcation diagrams only from time-waveforms, *Physica D: Nonlinear Phenomena* **79**, 348 (1994).
- [23] Y. Itoh, Y. Tada, and M. Adachi, Reconstructing bifurcation diagrams with lyapunov exponents from only time-series data using an extreme learning machine, *Nonlinear Theory and Its Applications, IEICE* **8**, 2 (2017).
- [24] Y. Itoh, S. Uenohara, M. Adachi, T. Morie, and K. Aihara, Reconstructing bifurcation diagrams only from time-series data generated by electronic circuits in discrete-time dynamical systems, *Chaos: An Interdisciplinary Journal of Nonlinear Science* **30**, 013128 (2020).
- [25] M. Hara and H. Kokubu, Learning dynamics by reservoir

- computing (in memory of prof. pavol brunovský), *Journal of Dynamics and Differential Equations* **36**, 515 (2024).
- [26] See Supplementary Material for networks with output bias and uniform distribution, the full rankness of the Gram matrix, the analytic solutions for NTK, the finiteness of the attractors for the bounded analytic NTK, the symmetries in learning period three, the bifurcation of characteristic attractors with the other network settings, the corresponding Lyapunov exponents, the finite-size effects in learning period three, learning period $n = 1, 2, 3, \dots$, and detailed discussion on the externalization of the latently existing unstable periods, which include Refs. [35, 40, 42–44, 48].
- [27] G.-B. Huang, Q.-Y. Zhu, and C.-K. Siew, Extreme learning machine: Theory and applications, *Neurocomputing* **70**, 489 (2006), neural Networks.
- [28] C. Saunders, A. Gammerman, and V. Vovk, Ridge regression learning algorithm in dual variables, in *Proceedings of the 15th International Conference on Machine Learning, ICML'98* (Morgan Kaufmann, San Francisco, CA, 1998) pp. 515–521.
- [29] J. Suykens, Nonlinear modelling and support vector machines, in *IMTC 2001. Proceedings of the 18th IEEE Instrumentation and Measurement Technology Conference. Rediscovering Measurement in the Age of Informatics (Cat. No.01CH 37188)*, Vol. 1 (2001) pp. 287–294 vol.1.
- [30] T. Liang and A. Rakhlin, Just interpolate: Kernel “ridgeless” regression can generalize, *The Annals of Statistics* **48**, 1329 (2020).
- [31] T. Hastie, A. Montanari, S. Rosset, and R. J. Tibshirani, Surprises in high-dimensional ridgeless least squares interpolation, *The Annals of Statistics* **50**, 949 (2022).
- [32] A. Jacot, F. Gabriel, and C. Hongler, Neural tangent kernel: Convergence and generalization in neural networks, in *Advances in Neural Information Processing Systems*, Vol. 31, edited by S. Bengio, H. Wallach, H. Larochelle, K. Grauman, N. Cesa-Bianchi, and R. Garnett (Curran Associates, Inc., 2018).
- [33] J. Lee, L. Xiao, S. Schoenholz, Y. Bahri, R. Novak, J. Sohl-Dickstein, and J. Pennington, Wide neural networks of any depth evolve as linear models under gradient descent, in *Advances in Neural Information Processing Systems*, Vol. 32, edited by H. Wallach, H. Larochelle, A. Beygelzimer, F. d'Alché-Buc, E. Fox, and R. Garnett (Curran Associates, Inc., 2019).
- [34] L. Carvalho, J. L. Costa, J. Mourão, and G. Oliveira, The positivity of the neural tangent kernel (2024), arXiv:2404.12928 [cs.LG].
- [35] S. Tamura and M. Tateishi, Capabilities of a four-layered feedforward neural network: four layers versus three, *IEEE Transactions on Neural Networks* **8**, 251 (1997).
- [36] M. Hermans and B. Schrauwen, Recurrent kernel machines: Computing with infinite echo state networks, *Neural Computation* **24**, 104 (2012).
- [37] J. Dong, R. Ohana, M. Rafayelyan, and F. Krzakala, Reservoir computing meets recurrent kernels and structured transforms, in *Advances in Neural Information Processing Systems*, Vol. 33, edited by H. Larochelle, M. Ranzato, R. Hadsell, M. Balcan, and H. Lin (Curran Associates, Inc., 2020) pp. 16785–16796.
- [38] J. Dong, E. Börve, M. Rafayelyan, and M. Unser, Asymptotic stability in reservoir computing, in *2022 International Joint Conference on Neural Networks (IJCNN)* (2022) pp. 01–08.
- [39] C. Williams, Computing with infinite networks, in *Advances in Neural Information Processing Systems*, Vol. 9, edited by M. Mozer, M. Jordan, and T. Petsche (MIT Press, 1996).
- [40] Y. Cho and L. Saul, Kernel methods for deep learning, in *Advances in Neural Information Processing Systems*, Vol. 22, edited by Y. Bengio, D. Schuurmans, J. Lafferty, C. Williams, and A. Culotta (Curran Associates, Inc., 2009).
- [41] W. De Melo and S. Van Strien, *One-Dimensional Dynamics* (Springer, Berlin, 1993).
- [42] S. v. Strien, T. Bedford, and H. Swift, Smooth dynamics on the interval (with an emphasis on quadratic-like maps), in *New Directions in Dynamical Systems*, London Mathematical Society Lecture Note Series (Cambridge University Press, 1988) p. 57–119.
- [43] S. Banerjee, J. A. Yorke, and C. Grebogi, Robust chaos, *Phys. Rev. Lett.* **80**, 3049 (1998).
- [44] S. Banerjee, M. Karthik, G. Yuan, and J. Yorke, Bifurcations in one-dimensional piecewise smooth maps-theory and applications in switching circuits, *IEEE Transactions on Circuits and Systems I: Fundamental Theory and Applications* **47**, 389 (2000).
- [45] H.-O. Peitgen, H. Jürgens, and D. Saupe, *Chaos and Fractals* (Springer New York, 2004).
- [46] A. Sharkovsky, Y. Maistrenko, and E. Romanenko, *Difference Equations and Their Applications*, Mathematics and Its Applications (Springer Netherlands, 2012).
- [47] G. Pastor, M. Romera, and F. Montoya, Harmonic structure of one-dimensional quadratic maps, *Phys. Rev. E* **56**, 1476 (1997).
- [48] C. Grebogi, E. Ott, and J. A. Yorke, Crises, sudden changes in chaotic attractors, and transient chaos, *Physica D: Nonlinear Phenomena* **7**, 181 (1983).
- [49] S. Ishihara and K. Kaneko, Magic number 7 ± 2 in networks of threshold dynamics, *Phys. Rev. Lett.* **94**, 058102 (2005).
- [50] S. Ortín, M. C. Soriano, L. Pesquera, D. Brunner, D. San-Martín, I. Fischer, C. R. Mirasso, and J. M. Gutiérrez, A unified framework for reservoir computing and extreme learning machines based on a single time-delayed neuron, *Scientific Reports* **5**, 14945 (2015).
- [51] K. Nakajima, Physical reservoir computing—an introductory perspective, *Japanese Journal of Applied Physics* **59**, 060501 (2020).
- [52] G. Marcucci, D. Pierangeli, and C. Conti, Theory of neuromorphic computing by waves: Machine learning by rogue waves, dispersive shocks, and solitons, *Phys. Rev. Lett.* **125**, 093901 (2020).
- [53] N. Akashi, Y. Kuniyoshi, S. Tsunegi, T. Taniguchi, M. Nishida, R. Sakurai, Y. Wakao, K. Kawashima, and K. Nakajima, A coupled spintronics neuromorphic approach for high-performance reservoir computing, *Advanced Intelligent Systems* **4**, 2200123 (2022).

Supplementary Material for “Thermodynamic Limit in Learning Period Three”

Yuichiro Terasaki^{1,*} and Kohei Nakajima^{2,3,†}

¹*Department of Mechano-Informatics, The University of Tokyo, Tokyo 113-8656, Japan*

²*Graduate School of Information Science and Technology,
The University of Tokyo, Tokyo 113-8656, Japan*

³*Next Generation Artificial Intelligence Research Center,
The University of Tokyo, Tokyo 113-8656, Japan*

(Dated: September 12, 2024)

This supplementary material describes the derivation procedures, calculations, numerical experiments, and additional figures in detail. We assign the numbers of equations, figures, and propositions here with S and specify the equations and figures by the same numbers in the main text.

CONTENTS

I. Thermodynamic Limit of the Learning Machine	2
A. Trained Network Output with Output Bias	2
B. Full Rankness of the Gram Matrix Θ	2
C. Analytic Solutions for Neural Tangent Kernels (NTKs)	3
D. Networks with Uniform Distributions	5
II. Finiteness of the Attractors of the Trained Map with the Bounded Analytic NTK	6
III. Symmetries in Learning Period Three	6
IV. Characteristic Attractors of the Trained Networks for $\phi = \text{erf}, \sin, \cos, \text{ReLU}$	10
V. Learning Period $n = 1, 2, 3, \dots$	15
VI. Externalization of the Latently Existing Unstable Periods	17
References	21

* terasaki@isi.imi.i.u-tokyo.ac.jp

† k-nakajima@isi.imi.i.u-tokyo.ac.jp

I. THERMODYNAMIC LIMIT OF THE LEARNING MACHINE

A. Trained Network Output with Output Bias

We define the neural network output $f_N(x)$ for an input $x \in \mathbb{R}$ as follows:

$$\begin{aligned} h_i(x) &\equiv W_i^{\text{in}}x + b_i^{\text{in}} \quad (i = 1, \dots, N), \\ f_N(x) &\equiv \frac{1}{\sqrt{N}} \sum_{i=1}^N W_i^{\text{out}} \phi(h_i(x)), \quad f_N^{\text{bias}}(x) \equiv \frac{1}{\sqrt{N}} \sum_{i=1}^N W_i^{\text{out}} \phi(h_i(x)) + b^{\text{out}}, \\ W_i^{\text{in}} &\sim \mathcal{N}(0, \sigma_w^2), \text{ and } b_i^{\text{in}} \sim \mathcal{N}(0, \sigma_b^2), \end{aligned} \quad (\text{S1})$$

where $W^{\text{in}} \in \mathbb{R}^{N \times 1}$ and $b^{\text{in}} \in \mathbb{R}^N$ are the input weights and biases randomly drawn from Gaussian distributions with zero mean and variance given by σ_w^2 and σ_b^2 , respectively; $\phi: \mathbb{R} \rightarrow \mathbb{R}$ is an activation function; and $W^{\text{out}} \in \mathbb{R}^{1 \times N}$ and $b^{\text{out}} \in \mathbb{R}$ are the output weights and bias optimized by ‘‘ridgeless’’ regression [1–7], respectively. As outlined in the main text, we consider specific activation functions (i.e., $\phi = \text{erf}, \sin, \cos, \text{ReLU}$) and use the following notations for all the target input–output pairs: \mathcal{D} , $|\mathcal{D}|$, \mathcal{X} , and \mathcal{Y} , where we denote the training dataset and its number by $\mathcal{D} \subseteq \mathbb{R} \times \mathbb{R}$ and $|\mathcal{D}|$, respectively, and use \mathcal{X} and \mathcal{Y} vectors to denote the input and output data. Note that by assuming that $\sigma_w = \sigma_b = \sigma$ and defining $W_0^{\text{out}} \equiv b^{\text{out}}$ and $\phi(h_0(x)) \equiv \sqrt{N}$, we can reduce this network model to that in the main text.

We obtained the thermodynamic limit of the trained network $f_\infty^*(x)$ as follows:

$$f_\infty^*(x) = \Theta(x, \mathcal{X}) \Theta^{-1} \mathcal{Y} = [\Theta(x, x_1) \ \cdots \ \Theta(x, x_{|\mathcal{D}|})] \begin{bmatrix} \Theta(x_1, x_1) & \cdots & \Theta(x_1, x_{|\mathcal{D}|}) \\ \vdots & \ddots & \vdots \\ \Theta(x_{|\mathcal{D}|}, x_1) & \cdots & \Theta(x_{|\mathcal{D}|}, x_{|\mathcal{D}|}) \end{bmatrix}^{-1} \begin{bmatrix} y_1 \\ \vdots \\ y_{|\mathcal{D}|} \end{bmatrix}, \quad (\text{S2})$$

where $\Theta(x, y) = \mathbb{E}[\phi(\omega x + \beta)\phi(\omega y + \beta)] = \frac{1}{2\pi\sigma_w\sigma_b} \int d\omega d\beta \phi(\omega x + \beta)\phi(\omega y + \beta) e^{-\frac{1}{2}\left(\frac{\omega^2}{\sigma_w^2} + \frac{\beta^2}{\sigma_b^2}\right)}$ and

$$\Theta^{\text{bias}}(x, y) = \mathbb{E}[\phi(\omega x + \beta)\phi(\omega y + \beta)] + 1 = \Theta(x, y) + 1.$$

We again assumed that the matrix Θ has full rank. Eq. (S2) indicates that if Θ has full rank, then Θ^{bias} also has full rank; however, we note that the existence of b^{out} does not ensure the full rank of Θ .

B. Full Rankness of the Gram Matrix Θ

In this subsection, we discuss the validity of the assumption of the full rankness of the matrix Θ based on the discussion in Ref. [8]. We suppose that the activation ϕ is continuous. Note that for the infinitely differentiable non-polynomial ϕ , the full rankness of the matrix $\hat{\Theta}$ (with finite N) is discussed in Ref. [1, 9]. As Θ is symmetric, it is necessary and sufficient to show that Θ is positive definite:

$$u^\top \Theta u = \mathbb{E} \left[\sum_{i=1}^{|\mathcal{D}|} \sum_{j=1}^{|\mathcal{D}|} u_i \phi(\omega x_i + \beta) \phi(\omega x_j + \beta) u_j \right] = \mathbb{E} \left[\left(\sum_{i=1}^{|\mathcal{D}|} u_i \phi(\omega x_i + \beta) \right)^2 \right] > 0 \quad (\text{S3})$$

for any non-zero $u \in \mathbb{R}^{|\mathcal{D}|} \setminus \{0\}$. From Eq. (S3), our assumption breaks down if and only if $u \neq 0$ satisfies

$$\sum_{i=1}^{|\mathcal{D}|} u_i \phi(\omega x_i + \beta) = 0 \quad (\text{S4})$$

for almost every $[\omega, \beta] \sim \mathcal{N}(\mathbf{0}, \sigma^2 I)$. Since $\mathcal{N}(\mathbf{0}, \sigma^2 I)$ has full support and ϕ is continuous, it is equivalent to

$$\sum_{i=1}^{|\mathcal{D}|} u_i \phi(W x_i + b) = 0, \text{ for every } [W, b] \in \mathbb{R}^2. \quad (\text{S5})$$

With the input data \mathcal{X} consisting of $|\mathcal{D}|$ distinct points, the following theorem states that if Eq. (S5) holds, then ϕ is a polynomial function.

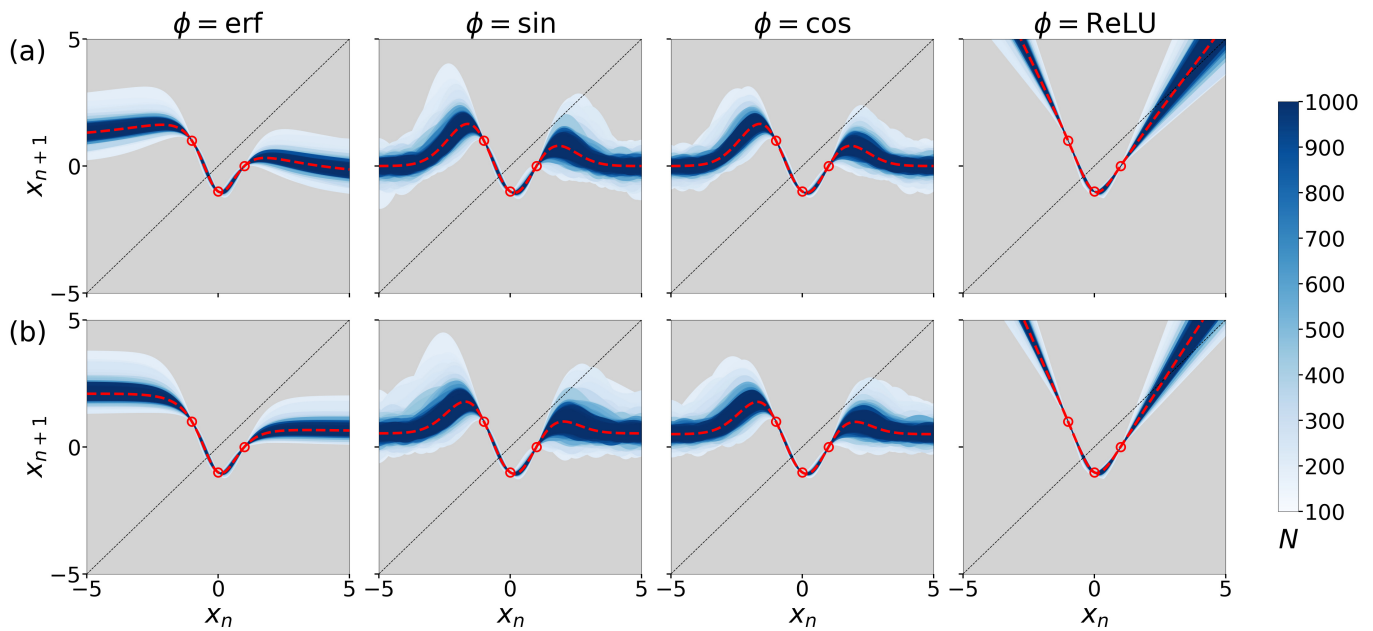


FIG. S1: Trained maps f_N^* for $\phi = \text{erf}, \sin, \cos, \text{ReLU}$ with the target period three $\mathcal{D} = \{-1, 1, 0\}$ and variances of the input parameters $\sigma_b^2 = \sigma_w^2 = 1.0$. The blue-colored areas indicate the maximum–minimum regions of f_N^* for 100 different realizations (a) without output bias or (b) with output bias. The red circles and the red dotted lines show the target period three and the thermodynamic limit f_∞^* , respectively. The darkness of blue corresponds to the number of nodes N , describing that regardless of the choice of ϕ , f_N^* degenerates into f_∞^* as N increases.

Theorem S1. (Ref. [8]) Let $z, w \in \mathbb{R}^D$ be totally non-aligned, meaning that

$$\begin{vmatrix} z_i & w_i \\ z_j & w_j \end{vmatrix} \neq 0, \text{ for all } i \neq j, \quad (\text{S6})$$

and let $\phi: \mathbb{R} \rightarrow \mathbb{R}$ be continuous. If there exists $u \in \mathbb{R}^D \setminus \{0\}$ such that

$$\sum_{i=1}^D u_i \phi(\theta_1 z_i + \theta_2 w_i) = 0, \text{ for every } [\theta_1, \theta_2] \in \mathbb{R}^2, \quad (\text{S7})$$

then ϕ is a polynomial function.

Therefore, our assumption is valid in learning period $n = 1, 2, 3, \dots$ as long as the activation ϕ is a non-polynomial continuous function.

C. Analytic Solutions for Neural Tangent Kernels (NTKs)

In this subsection, we provide the analytic solutions of $\Theta(x, y)$ for the activation functions $\phi = \text{erf}, \sin, \cos, \text{ReLU}$. Following Williams [10], the NTK for $\phi = \text{erf}$ is given by

$$\Theta^{\text{erf}}(x, y) = \frac{2}{\pi} \arcsin \frac{2(\sigma_b^2 + \sigma_w^2 xy)}{\sqrt{[1 + 2(\sigma_b^2 + \sigma_w^2 x^2)][1 + 2(\sigma_b^2 + \sigma_w^2 y^2)]}}. \quad (\text{S8})$$

Following Cho and Saul [11], the NTK for $\phi = \text{ReLU}$ is given by

$$\Theta^{\text{relu}}(x, y) = \frac{1}{2\pi} \sqrt{(\sigma_b^2 + \sigma_w^2 x^2)(\sigma_b^2 + \sigma_w^2 y^2)} \left\{ \sqrt{1 - \frac{(\sigma_b^2 + \sigma_w^2 xy)^2}{(\sigma_b^2 + \sigma_w^2 x^2)(\sigma_b^2 + \sigma_w^2 y^2)}} + \frac{(\pi - \psi)(\sigma_b^2 + \sigma_w^2 xy)}{\sqrt{(\sigma_b^2 + \sigma_w^2 x^2)(\sigma_b^2 + \sigma_w^2 y^2)}} \right\}, \quad (\text{S9})$$

where $\psi \equiv \arccos \frac{\sigma_b^2 + \sigma_w^2 xy}{\sqrt{(\sigma_b^2 + \sigma_w^2 x^2)(\sigma_b^2 + \sigma_w^2 y^2)}}$.

Here, $0 \leq \psi \leq \pi$ is an angle between the vectors $[\sigma_b, \sigma_w x], [\sigma_b, \sigma_w y] \in \mathbb{R}^2$, indicating the similarity between x and y . Below, we derive NTKs for $\phi = \sin, \cos$. Using the formulae $\sin(\omega x + \beta) \sin(\omega y + \beta) = \{\cos[\omega(x - y)] - \cos[\omega(x + y) + 2\beta]\}/2$ and $\cos(\omega x + \beta) \cos(\omega y + \beta) = \{\cos[\omega(x - y)] + \cos[\omega(x + y) + 2\beta]\}/2$, we get

$$\Theta^{\sin}(x, y) = I_1 - I_2, \quad \Theta^{\cos}(x, y) = I_1 + I_2,$$

$$\text{where } I_1 \equiv \frac{1}{4\pi\sigma_w\sigma_b} \int d\omega d\beta \cos[\omega(x - y)] e^{-\frac{1}{2}\left(\frac{\omega^2}{\sigma_w^2} + \frac{\beta^2}{\sigma_b^2}\right)} \text{ and } I_2 \equiv \frac{1}{4\pi\sigma_w\sigma_b} \int d\omega d\beta \cos[\omega(x + y) + 2\beta] e^{-\frac{1}{2}\left(\frac{\omega^2}{\sigma_w^2} + \frac{\beta^2}{\sigma_b^2}\right)}. \quad (\text{S10})$$

Applying the Gaussian integral formula to I_1 and I_2 in Eq. (S10), we get

$$\begin{aligned} I_1 &= \frac{1}{4\pi\sigma_w\sigma_b} \int_{-\infty}^{\infty} d\beta e^{-\frac{\beta^2}{2\sigma_b^2}} \int_{-\infty}^{\infty} d\omega \cos[\omega(x - y)] e^{-\frac{\omega^2}{2\sigma_w^2}} \\ &= \frac{1}{2\sqrt{2\pi}\sigma_w} \int_{-\infty}^{\infty} d\omega \cos[\omega(x - y)] e^{-\frac{\omega^2}{2\sigma_w^2}} = \frac{1}{2\sqrt{2\pi}\sigma_w} \text{Re} \left[\int_{-\infty}^{\infty} d\omega e^{-\frac{\omega^2}{2\sigma_w^2} + i\omega(x-y)} \right] = \frac{e^{-\frac{\sigma_w^2}{2}(x-y)^2}}{2}, \text{ and} \end{aligned} \quad (\text{S11})$$

$$I_2 = \frac{1}{2} \text{Re} \left[\frac{1}{\sqrt{2\pi}\sigma_b} \int_{-\infty}^{\infty} d\beta e^{-\frac{\beta^2}{2\sigma_b^2} + 2i\beta} \frac{1}{\sqrt{2\pi}\sigma_w} \int_{-\infty}^{\infty} d\omega e^{-\frac{\omega^2}{2\sigma_w^2} + i\omega(x+y)} \right] = \frac{e^{-\frac{\sigma_w^2}{2}(x+y)^2 - 2\sigma_b^2}}{2}, \quad (\text{S12})$$

where Re is the real-part operator. Substituting Eqs. (S11)–(S12) into Eq. (S10), we obtain the following formulae for the NTKs for $\phi = \sin, \cos$:

$$\Theta^{\sin}(x, y) = \frac{1}{2} \left\{ e^{-\frac{\sigma_w^2}{2}(x-y)^2} - e^{-\frac{\sigma_w^2}{2}(x+y)^2 - 2\sigma_b^2} \right\} \text{ and } \Theta^{\cos}(x, y) = \frac{1}{2} \left\{ e^{-\frac{\sigma_w^2}{2}(x-y)^2} + e^{-\frac{\sigma_w^2}{2}(x+y)^2 - 2\sigma_b^2} \right\}. \quad (\text{S13})$$

We note that the kernels Eqs. (S8), (S9), and (S13) are invariant under the swapping of x and y and that $-1 \leq \Theta(x, y) \leq 1$ for $\phi = \text{erf}, \sin, \cos$, since NTK is the expectation of the product of the activation functions (Eq. (S2)).

If $\sigma_b = \sigma_w = \sigma$, we obtain

$$\Theta^{\text{erf}}(x, y) = \frac{2}{\pi} \arcsin \frac{2\sigma^2(1 + xy)}{\sqrt{[1 + 2\sigma^2(1 + x^2)][1 + 2\sigma^2(1 + y^2)]}}, \quad (\text{13})$$

$$\Theta^{\sin}(x, y) = \frac{1}{2} \left\{ e^{-\frac{\sigma^2}{2}(x-y)^2} - e^{-\frac{\sigma^2}{2}(x+y)^2 - 2\sigma^2} \right\}, \quad (\text{S14})$$

$$\Theta^{\cos}(x, y) = \frac{1}{2} \left\{ e^{-\frac{\sigma^2}{2}(x-y)^2} + e^{-\frac{\sigma^2}{2}(x+y)^2 - 2\sigma^2} \right\}, \text{ and} \quad (\text{S15})$$

$$\Theta^{\text{relu}}(x, y) = \frac{\sigma^2}{2\pi} \sqrt{(1 + x^2)(1 + y^2)} \left\{ \sqrt{1 - \frac{(1 + xy)^2}{(1 + x^2)(1 + y^2)}} + (\pi - \psi) \frac{1 + xy}{\sqrt{(1 + x^2)(1 + y^2)}} \right\}, \quad (\text{S16})$$

$$\text{where } \psi \equiv \arccos \frac{1 + xy}{\sqrt{(1 + x^2)(1 + y^2)}}.$$

The formulae for $\frac{\partial \Theta}{\partial x}(x, y)$ for $\phi = \text{erf}, \sin, \cos, \text{ReLU}$ are therefore given by

$$\frac{\partial \Theta^{\text{erf}}}{\partial x}(x, y) = \frac{4\sigma^2}{\pi [1 + 2\sigma^2(1 + x^2)]} \frac{y - 2\sigma^2(x - y)}{\sqrt{1 + 2\sigma^2(2 + x^2 + y^2) + 4\sigma^4(x - y)^2}}, \quad (\text{S17})$$

$$\frac{\partial \Theta^{\sin}}{\partial x}(x, y) = -\frac{\sigma^2}{2} \left\{ (x - y)e^{-\frac{\sigma^2}{2}(x-y)^2} - (x + y)e^{-\frac{\sigma^2}{2}(x+y)^2 - 2\sigma^2} \right\}, \quad (\text{S18})$$

$$\frac{\partial \Theta^{\cos}}{\partial x}(x, y) = -\frac{\sigma^2}{2} \left\{ (x - y)e^{-\frac{\sigma^2}{2}(x-y)^2} + (x + y)e^{-\frac{\sigma^2}{2}(x+y)^2 - 2\sigma^2} \right\}, \text{ and} \quad (\text{S19})$$

$$\frac{\partial \Theta^{\text{relu}}}{\partial x}(x, y) = \frac{\sigma^2}{2\pi} \left\{ \frac{x|x - y|}{1 + x^2} + (\pi - \psi)y \right\}, \quad (\text{S20})$$

$$\text{where } \psi \equiv \arccos \frac{1 + xy}{\sqrt{(1 + x^2)(1 + y^2)}}.$$

Eq. (S16) indicates that for $\phi = \text{ReLU}$, varying σ has little effect on the trained network output (Eq. (8)). The effect disappears in the absence of b^{out} , and increasing σ diminishes the efficacy of b^{out} in $f_{\infty}^{*, \text{bias}}$ ($f_{\infty}^{*, \text{bias}} \rightarrow f_{\infty}^*$).

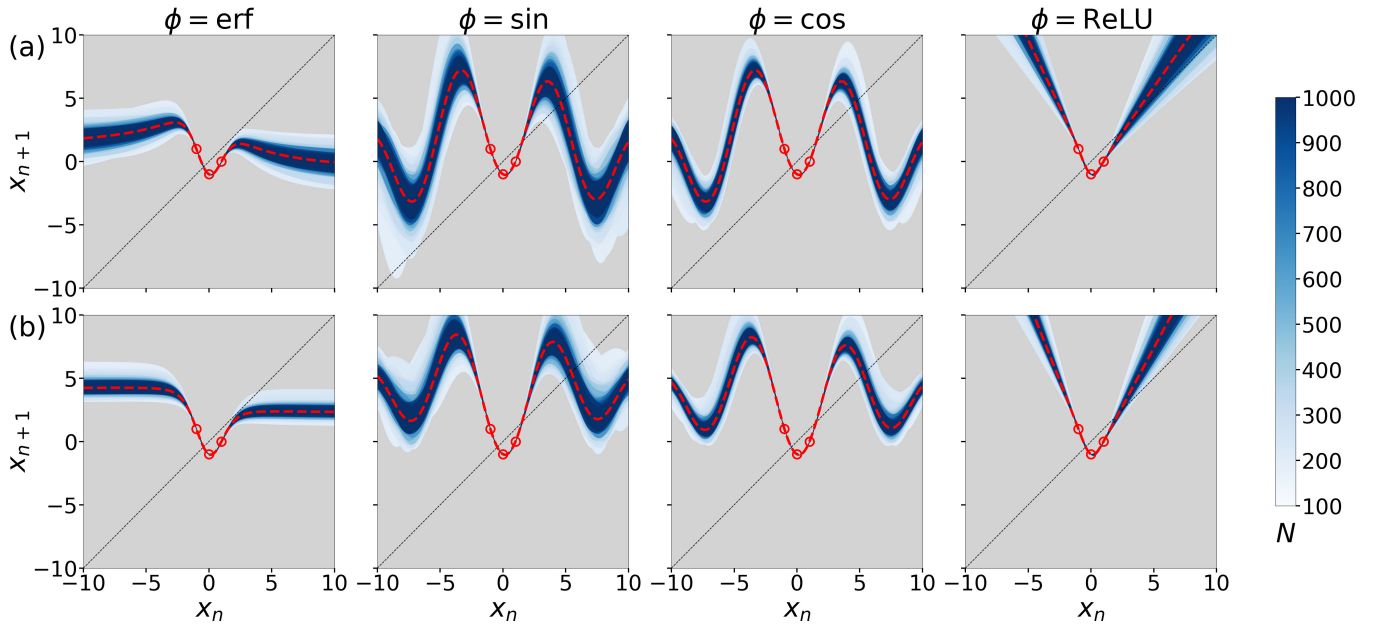


FIG. S2: Trained maps f_N^* with the input parameters drawn from uniform distributions in the same setting as in Fig. S1. The choice of the probability distribution of the input layer affects the shape of the trained maps, in which we observe a significant effect for $\phi = \sin, \cos$.

Fig. S1 shows the shape of the trained map for each activation function and how the trained network with a finite number of nodes degenerates into its unique thermodynamic limit. We observe that the choice of ϕ and the existence of b^{out} affect the shapes of the trained maps. In particular, the behavior of $f_\infty^*(x)$ for a large input $|x| \gg 1$ depends strongly on the nonlinearity of the network. For $\phi = \text{erf}, \sin, \cos$, the kernels $\Theta(x, y)$, and therefore, $f_\infty^*(x)$, converge to constant values as $x \rightarrow \pm\infty$:

$$\lim_{x \rightarrow \pm\infty} \Theta^{\text{erf}}(x, y) = \begin{cases} \frac{2}{\pi} \arcsin \frac{y\sqrt{2\sigma^2}}{\sqrt{1+2\sigma^2(1+y^2)}} & (x \rightarrow +\infty) \\ -\frac{2}{\pi} \arcsin \frac{y\sqrt{2\sigma^2}}{\sqrt{1+2\sigma^2(1+y^2)}} & (x \rightarrow -\infty) \end{cases} \quad \text{and} \quad (\text{S21})$$

$$\lim_{x \rightarrow \pm\infty} \Theta^{\sin}(x, y) = \lim_{x \rightarrow \pm\infty} \Theta^{\cos}(x, y) = 0. \quad (\text{S22})$$

Eq. (S22) indicates that regardless of the value of σ , the trained network output $f_\infty^*(x)$ decreases to zero if x deviates significantly from the target data \mathcal{D} . In contrast, $f_\infty^*(x)$ for $\phi = \text{ReLU}$ diverges as $x \rightarrow \pm\infty$.

D. Networks with Uniform Distributions

The kernel $\hat{\Theta}(x, y)$ (Eq. (4)), with the input parameters drawn from the following uniform distributions:

$$W_i^{\text{in}} \sim \mathcal{U}(-\sigma_w, \sigma_w) \text{ and } b_i^{\text{in}} \sim \mathcal{U}(-\sigma_b, \sigma_b), \quad (\text{S23})$$

also converges in probability to $\Theta(x, y)$ —that is the expectation over random variables $\omega \sim \mathcal{U}(-\sigma_w, \sigma_w)$ and $\beta \sim \mathcal{U}(-\sigma_b, \sigma_b)$ —in the limit $N \rightarrow \infty$ by the law of large numbers:

$$\hat{\Theta}(x, y) \rightarrow \Theta(x, y) = \mathbb{E}[\phi(\omega x + \beta)\phi(\omega y + \beta)] = \frac{1}{4\sigma_w\sigma_b} \int_{-\sigma_b}^{\sigma_b} d\beta \int_{-\sigma_w}^{\sigma_w} d\omega \phi(\omega x + \beta)\phi(\omega y + \beta) \quad \text{and} \quad (\text{S24})$$

$$\hat{\Theta}^{\text{bias}}(x, y) \rightarrow \Theta^{\text{bias}}(x, y) = \Theta(x, y) + 1.$$

As Eq. (S24) is a definite integral, we can numerically compute NTK. Therefore, assuming that the matrix Θ has full rank, we can compute $f_\infty^*(x)$ for any input x (Fig. S2).

II. FINITENESS OF THE ATTRACTORS OF THE TRAINED MAP WITH THE BOUNDED ANALYTIC NTK

The following theorem restricts the number of the attractors of a smooth map from a finite interval I to itself [12]:

Theorem S2. (Melo–Strien) *If $f : I \rightarrow I$ is a C^2 map with non-flat critical points, then there exist $\lambda > 1$ and $n_0 \in \mathbb{N}$ such that*

$$\left| \frac{d}{dx} f^n(p) \right| > \lambda \quad (\text{S25})$$

for every periodic point p of f of period $n \geq n_0$.

Here, we say that $c \in I$ is a critical point if it satisfies $\frac{d}{dx} f(c) = 0$ and that a critical point c for a smooth map is non-flat if there exists $k \geq 2$ such that $\frac{d^k}{dx^k} f(c) \neq 0$ [12, 13]. Note that if f is a non-constant analytic map with critical points, then all the critical points are non-flat, since $f(x)$ has the Taylor expansion for every $x_0 \in I$, and its coefficients for some $k \geq 2$ degrees are non-zero [13]. Hence, we obtain the following corollary of Theorem S2:

Corollary S3. *If $f : I \rightarrow I$ is a non-constant analytic map with critical points, then there exist $\lambda > 1$ and $n_0 \in \mathbb{N}$ such that*

$$\left| \frac{d}{dx} f^n(p) \right| > \lambda \quad (\text{S26})$$

for every periodic point p of f of period $n \geq n_0$.

For our neural network model, if the kernels $\hat{\Theta}(x, y)$ and $\Theta(x, y)$ are bounded and analytic (e.g., if $\phi = \text{erf}, \sin, \cos$), then the network outputs are also bounded and analytic, since $f_N^*(x)$ (Eq. (6)) and $f_\infty^*(x)$ (Eq. (8)) are described by the weighted sum of the kernels. Furthermore, in learning period $n \geq 2$, $f_N^*(x)$ and $f_\infty^*(x)$, with full-rank matrices $\hat{\Theta}$ and Θ , respectively, cannot be constant functions because, otherwise, they will not be able to replicate the target input–output pairs \mathcal{D} . In addition, in learning period three (LP3), according to Rolle’s theorem, f_N^* and f_∞^* have at least one critical point by their folding around \mathcal{D} ; thus, we can restrict the bounded f_N^* and f_∞^* to some finite interval that contains all the periods and critical points. Therefore, with the full-rank Gram matrix and the bounded and analytic kernel, f_N^* and f_∞^* in LP3 has, at most, finitely many stable periods (attractors) based on Corollary S3.

III. SYMMETRIES IN LEARNING PERIOD THREE

In this section, we state that the bifurcation of characteristic attractors in LP3 ($\mathcal{D} = \{a, b, c\}$) has two types of universal symmetry properties derived from the symmetry of $\{a, b, c\}$ under the swapping of a and b (Fig. S3). For the sake of simplicity, we assume that $a < b$, with a and b fixed. One symmetry is the inverted structure near the singular points $c = a$ and $c = b$:

$$\lim_{c \nearrow a} f_\infty^*(x)|_{\mathcal{D}=\{a,b,c\}} = \lim_{c \searrow a} f_\infty^*(x)|_{\mathcal{D}=\{b,a,c\}} \quad \text{and} \quad \lim_{c \nearrow b} f_\infty^*(x)|_{\mathcal{D}=\{a,b,c\}} = \lim_{c \searrow b} f_\infty^*(x)|_{\mathcal{D}=\{b,a,c\}}. \quad (\text{S27})$$

The left-hand side of Eq. (S27) corresponds to the outside structure ($c < a$ or $b < c$), and the right-hand side of the same equation corresponds to the inside structure ($a < c < b$), with the other type of target period three (Fig. S4). The other symmetry is, for the specific case of $b \approx -a$ and $\Theta(x, y) = \Theta(-x, -y)$, the inversion of the whole bifurcation structure under the swapping of a and b :

$$f_\infty^*(x)|_{\mathcal{D}=\{a,b,c\}} \simeq -f_\infty^*(-x + a + b)|_{\mathcal{D}=\{b,a,-c+a+b\}} + a + b, \quad (\text{S28})$$

where the symbol \simeq means that the shapes of the two maps are similar when $b \approx -a$ (Fig. S5). The assumption that $\Theta(x, y) = \Theta(-x, -y)$ is valid if the distribution of W^{in} is symmetric at $W^{\text{in}} = 0$ (see Sec. VI). Note that the following equation always holds for target period three even if $\Theta(x, y) \neq \Theta(-x, -y)$:

$$f_\infty^*(p)|_{\mathcal{D}=\{a,b,c\}} = -f_\infty^*(-p + a + b)|_{\mathcal{D}=\{b,a,-c+a+b\}} + a + b \quad (p = a, b, c). \quad (\text{S29})$$

By combining these two symmetries (Eqs. (S27) and (S28)), we can qualitatively infer the outside structure only from the bifurcation diagram in the inside region if $b \approx -a$ (Fig. 2(a),(b)).

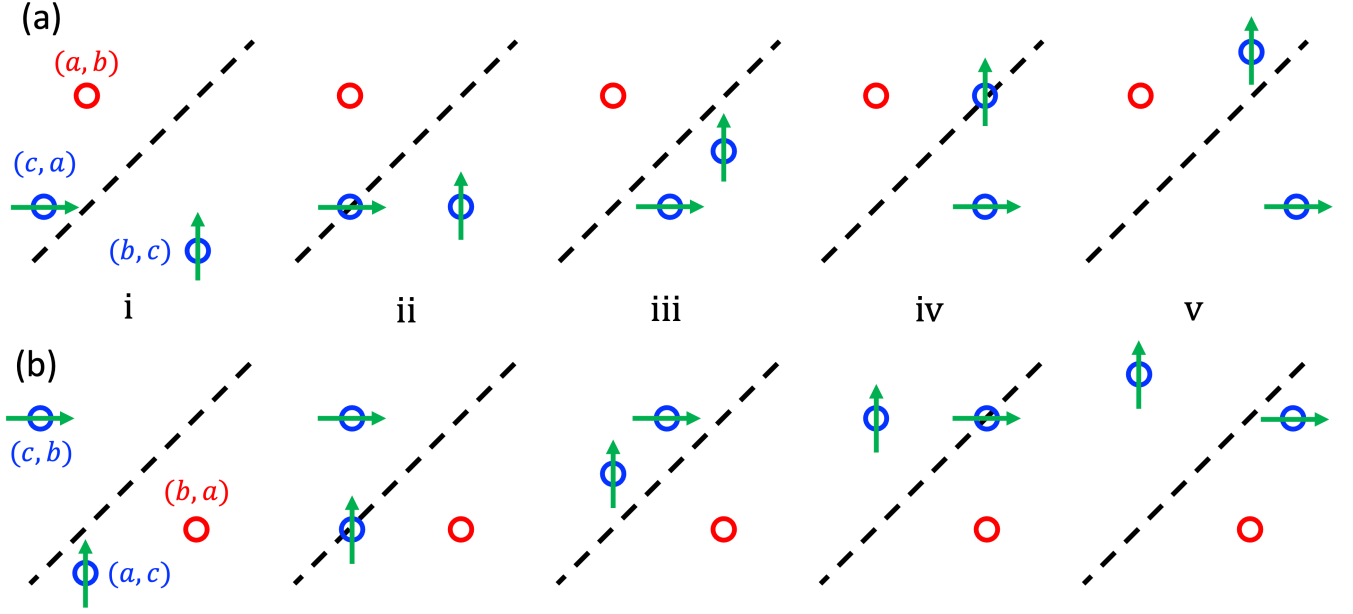


FIG. S3: Symmetry of target period three. (a) $\mathcal{D} = \{a, b, c\}$. (b) $\mathcal{D} = \{b, a, c\}$. The five regions (i)–(v) show the return maps in (i) $c < a$, (ii) $c = a$, (iii) $a < c < b$, (iv) $c = b$, and (v) $b < c$, respectively. The dotted lines correspond to $x_{n+1} = x_n$. The circles indicate target period three, and the red circles indicate a c -independent point (a, b) or (b, a) . The green arrows represent the moving direction of \mathcal{D} as c increases. The one-to-one correspondences (a)(ii)–(b)(ii) and (a)(iv)–(b)(iv) create the symmetry in Eq. (S27). Rotating the plots in (b) by 180 degrees around $(\frac{a+b}{2}, \frac{a+b}{2})$ and transforming c to $-c + a + b$ produces the same plots as in (a) (Eq. (S29)).

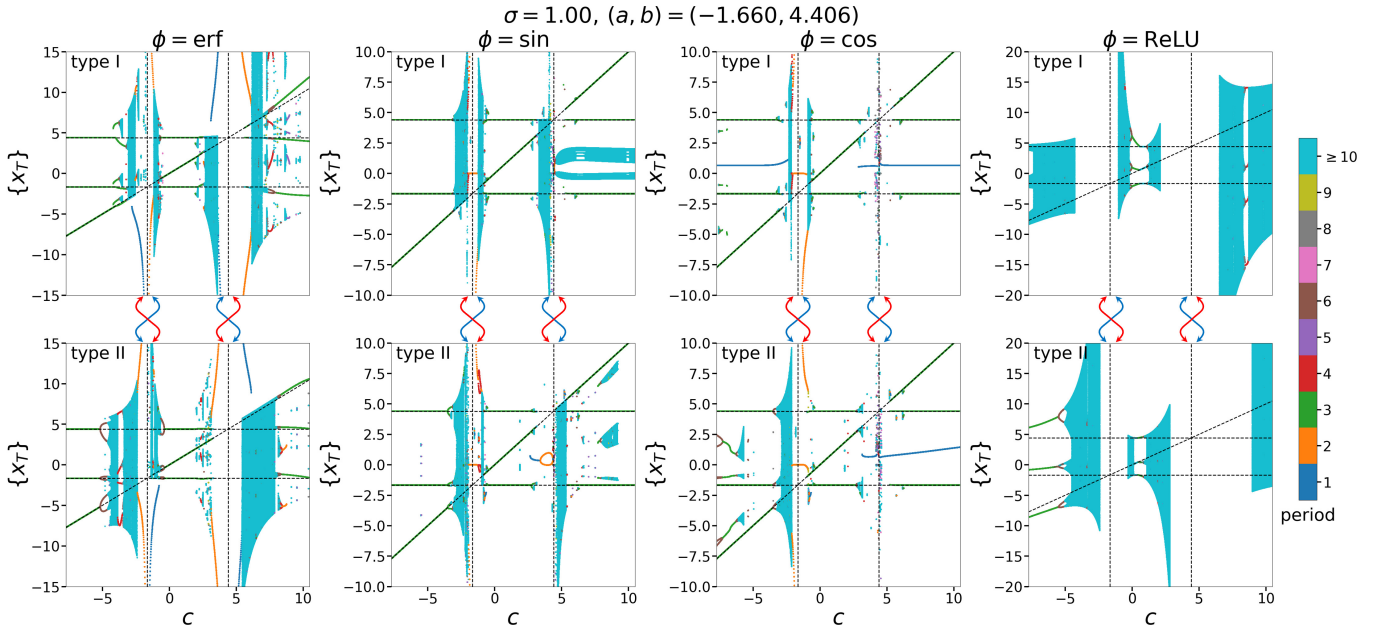


FIG. S4: Symmetry in Eq. (S27). Bifurcation of characteristic attractors of the dynamical systems $f_{\infty}^*|_{\mathcal{D}=\{a,b,c\}}$ (type I) and $f_{\infty}^*|_{\mathcal{D}=\{b,a,c\}}$ (type II) with respect to c . The dotted lines indicate target period three; the diagonal lines correspond to a varying c . The red arrows indicate the qualitative correspondence between the outside structure ($c < a$ or $b < c$) of type I and the inside structure ($a < c < b$) of type II; and the blue arrows indicate the qualitative correspondence between the outside structure ($c < a$ or $b < c$) of type II and the inside structure ($a < c < b$) of type I.

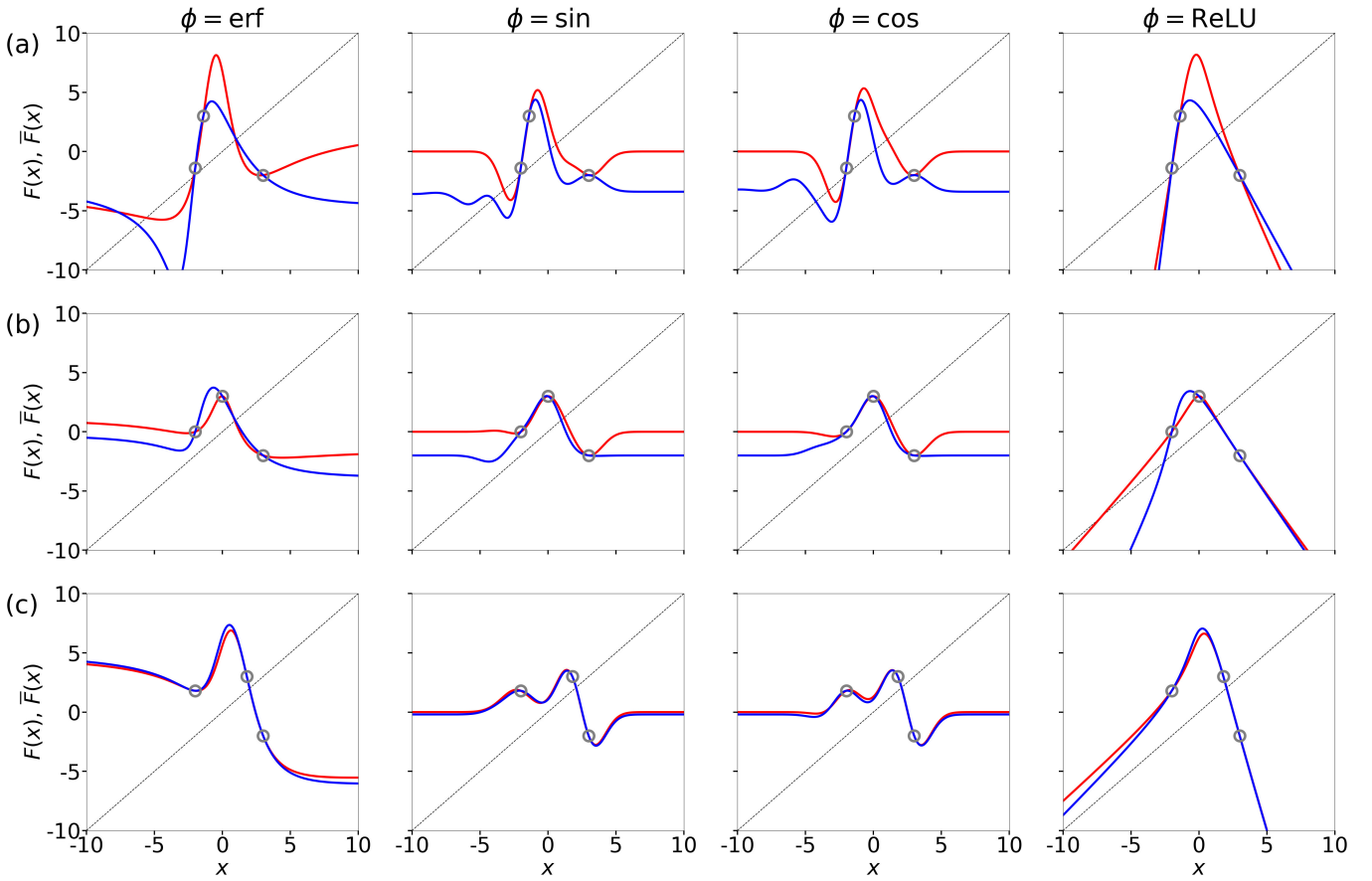


FIG. S5: Symmetry of Eq. (S28). $\{a, b, c\} =$ (a) $\{-2.0, -1.2, 3.0\}$, (b) $\{-2.0, 0.0, 3.0\}$, and (c) $\{-2.0, 1.8, 3.0\}$, with the fixed scale of weights $\sigma = 1.0$. The circles indicate target period three. The red and blue lines indicate $F(x) \equiv f_{\infty}^*(x)|_{\mathcal{D}=\{a,b,c\}}$ and $\bar{F}(x) \equiv -f_{\infty}^*(-x+a+b)|_{\mathcal{D}=\{b,a,-c+a+b\}} + a+b$, respectively. As b approaches $-a$, the symmetry around $x = a, b, c$ (Eq. (S29)) spreads throughout $x \in \mathbb{R}$ (Eq. (S36)) if $\Theta(x, y) = \Theta(-x, -y)$.

Below, we show the proof of Eq. (S28), restricted to the case of $b = -a$. Combining Eq. (8) with $\Theta(x, y) = \Theta(y, x)$, $f_{\infty}^*(x)|_{\mathcal{D}=\{a,b,c\}}$ is given by

$$\begin{aligned}
 f_{\infty}^*(x)|_{\mathcal{D}=\{a,b,c\}} = & \frac{b}{|\Theta|} [\Theta(x, a) \{ \Theta(b, b)\Theta(c, c) - \Theta(b, c)^2 \} \\
 & + \Theta(x, b) \{ \Theta(b, c)\Theta(c, a) - \Theta(a, b)\Theta(c, c) \} \\
 & + \Theta(x, c) \{ \Theta(a, b)\Theta(b, c) - \Theta(b, b)\Theta(c, a) \}] \\
 & + \frac{c}{|\Theta|} [\Theta(x, a) \{ \Theta(b, c)\Theta(c, a) - \Theta(a, b)\Theta(c, c) \} \\
 & + \Theta(x, b) \{ \Theta(c, c)\Theta(a, a) - \Theta(c, a)^2 \} \\
 & + \Theta(x, c) \{ \Theta(a, b)\Theta(c, a) - \Theta(a, a)\Theta(b, c) \}] \\
 & + \frac{a}{|\Theta|} [\Theta(x, a) \{ \Theta(a, b)\Theta(b, c) - \Theta(b, b)\Theta(c, a) \} \\
 & + \Theta(x, b) \{ \Theta(a, b)\Theta(c, a) - \Theta(a, a)\Theta(b, c) \} \\
 & + \Theta(x, c) \{ \Theta(a, a)\Theta(b, b) - \Theta(a, b)^2 \}] \text{ and}
 \end{aligned} \tag{S30}$$

$$|\Theta| = \Theta(a, a)\Theta(b, b)\Theta(c, c) + 2\Theta(a, b)\Theta(b, c)\Theta(c, a) - \Theta(a, a)\Theta(b, c)^2 - \Theta(b, b)\Theta(c, a)^2 - \Theta(c, c)\Theta(a, b)^2. \tag{S31}$$

Applying $b = -a$ and $\Theta(x, y) = \Theta(-x, -y)$ to both Eqs. (S30) and (S31) yields the following equations:

$$\begin{aligned}
f_{\infty}^*(x)|_{\mathcal{D}=\{a,-a,c\}} &= -\frac{a}{|\Theta|} [\Theta(x, a) \{\Theta(a, a)\Theta(c, c) - \Theta(c, -a)^2\} \\
&\quad + \Theta(x, -a) \{\Theta(c, -a)\Theta(c, a) - \Theta(a, -a)\Theta(c, c)\} \\
&\quad + \Theta(x, c) \{\Theta(a, -a)\Theta(c, -a) - \Theta(a, a)\Theta(c, a)\}] \\
&\quad + \frac{c}{|\Theta|} [\Theta(x, a) \{\Theta(c, -a)\Theta(c, a) - \Theta(a, -a)\Theta(c, c)\} \\
&\quad + \Theta(x, -a) \{\Theta(c, c)\Theta(a, a) - \Theta(c, a)^2\} \\
&\quad + \Theta(x, c) \{\Theta(a, -a)\Theta(c, a) - \Theta(a, a)\Theta(c, -a)\}] \\
&\quad + \frac{a}{|\Theta|} [\Theta(x, a) \{\Theta(a, -a)\Theta(c, -a) - \Theta(a, a)\Theta(c, a)\} \\
&\quad + \Theta(x, -a) \{\Theta(a, -a)\Theta(c, a) - \Theta(a, a)\Theta(c, -a)\} \\
&\quad + \Theta(x, c) \{\Theta(a, a)^2 - \Theta(a, -a)^2\}] \text{ and}
\end{aligned} \tag{S32}$$

$$|\Theta| = \Theta(a, a)^2\Theta(c, c) + 2\Theta(a, -a)\Theta(c, a)\Theta(c, -a) - \Theta(a, a) \{\Theta(c, a)^2 + \Theta(c, -a)^2\} - \Theta(c, c)\Theta(a, -a)^2. \tag{S33}$$

We note that $|\Theta|$ (Eq. (S33)) is invariant under the sign change of a or c ($a \rightarrow -a$ and $c \rightarrow -c$). Now, let us consider the other type of LP3 ($\mathcal{D} = \{-a, a, c\}$), that is, the sign change of a :

$$\begin{aligned}
f_{\infty}^*(x)|_{\mathcal{D}=\{-a,a,c\}} &= \frac{a}{|\Theta|} [\Theta(x, -a) \{\Theta(a, a)\Theta(c, c) - \Theta(c, a)^2\} \\
&\quad + \Theta(x, a) \{\Theta(c, a)\Theta(c, -a) - \Theta(a, -a)\Theta(c, c)\} \\
&\quad + \Theta(x, c) \{\Theta(a, -a)\Theta(c, a) - \Theta(a, a)\Theta(c, -a)\}] \\
&\quad + \frac{c}{|\Theta|} [\Theta(x, -a) \{\Theta(c, a)\Theta(c, -a) - \Theta(a, -a)\Theta(c, c)\} \\
&\quad + \Theta(x, a) \{\Theta(c, c)\Theta(a, a) - \Theta(c, -a)^2\} \\
&\quad + \Theta(x, c) \{\Theta(a, -a)\Theta(c, -a) - \Theta(a, a)\Theta(c, a)\}] \\
&\quad - \frac{a}{|\Theta|} [\Theta(x, -a) \{\Theta(a, -a)\Theta(c, a) - \Theta(a, a)\Theta(c, -a)\} \\
&\quad + \Theta(x, a) \{\Theta(a, -a)\Theta(c, -a) - \Theta(a, a)\Theta(c, a)\} \\
&\quad + \Theta(x, c) \{\Theta(a, a)^2 - \Theta(a, -a)^2\}].
\end{aligned} \tag{S34}$$

Applying the transformation $x \rightarrow -x$ and $c \rightarrow -c$ to Eq. (S34), we obtain

$$\begin{aligned}
f_{\infty}^*(-x)|_{\mathcal{D}=\{-a,a,-c\}} &= \frac{a}{|\Theta|} [\Theta(x, a) \{\Theta(a, a)\Theta(c, c) - \Theta(c, -a)^2\} \\
&\quad + \Theta(x, -a) \{\Theta(c, -a)\Theta(c, a) - \Theta(a, -a)\Theta(c, c)\} \\
&\quad + \Theta(x, c) \{\Theta(a, -a)\Theta(c, -a) - \Theta(a, a)\Theta(c, a)\}] \\
&\quad - \frac{c}{|\Theta|} [\Theta(x, a) \{\Theta(c, -a)\Theta(c, a) - \Theta(a, -a)\Theta(c, c)\} \\
&\quad + \Theta(x, -a) \{\Theta(c, c)\Theta(a, a) - \Theta(c, a)^2\} \\
&\quad + \Theta(x, c) \{\Theta(a, -a)\Theta(c, a) - \Theta(a, a)\Theta(c, -a)\}] \\
&\quad - \frac{a}{|\Theta|} [\Theta(x, a) \{\Theta(a, -a)\Theta(c, -a) - \Theta(a, a)\Theta(c, a)\} \\
&\quad + \Theta(x, -a) \{\Theta(a, -a)\Theta(c, a) - \Theta(a, a)\Theta(c, -a)\} \\
&\quad + \Theta(x, c) \{\Theta(a, a)^2 - \Theta(a, -a)^2\}].
\end{aligned} \tag{S35}$$

Eqs. (S32) and (S35) yield

$$f_{\infty}^*(x)|_{\mathcal{D}=\{a,-a,c\}} = -f_{\infty}^*(-x)|_{\mathcal{D}=\{-a,a,-c\}}, \tag{S36}$$

which is what we wanted to prove. Thus, $f_{\infty}^*(x)|_{\mathcal{D}=\{a,-a,c\}}$ is topologically conjugate to $f_{\infty}^*(x)|_{\mathcal{D}=\{-a,a,-c\}}$ if $\Theta(x, y) = \Theta(-x, -y)$.

IV. CHARACTERISTIC ATTRACTORS OF THE TRAINED NETWORKS FOR $\phi = \text{erf}, \text{sin}, \text{cos}, \text{ReLU}$

In this section, we show the bifurcation of characteristic attractors in LP3 for $\phi = \text{erf}, \text{sin}, \text{cos}, \text{ReLU}$ and discuss how the choice of \mathcal{D} , ϕ , and σ affects the characteristic attractors. Hereafter, we only analyze the bifurcation in $a < c < -a$ with $\mathcal{D} = \{a, -a, c\}$, considering the symmetry properties of Eqs. (S27) and (S28).

Figures S6 and S7 show the one-dimensional bifurcation diagrams with respect to c , and Figs. S8, S9, and S10 show the two-dimensional bifurcation diagrams with respect to c and σ . The nonlinearity ϕ changes the dependence of f_∞^* (or $f_\infty^{*,\text{bias}}$) on \mathcal{D} and σ , resulting in the broad diversity of the bifurcation of characteristic attractors. We note that for $\phi = \text{sin}, \text{cos}$, the wavy deviations of f_N^* from f_∞^* cause the large difference in the embeddable attractors (Figs. S10 and S11).

For $\phi = \text{ReLU}$, the σ -dependence of NTK (Eq.(S16)) is canceled out, resulting in the uniform bifurcation structure along the σ -direction. In contrast, varying σ dramatically changes the bifurcation for $\phi = \text{erf}, \text{sin}, \text{cos}$; the target orbit \mathcal{D} tends to be locally stable as σ increases (the black-hatched areas in Figs. S8 and S9) because the derivative of NTK at data point y approaches zero for a large σ :

$$\frac{\partial \Theta^{\text{erf}}}{\partial x}(y, y) = \frac{4\sigma^2 y}{\pi [1 + 2\sigma^2(1 + y^2)] \sqrt{1 + 4\sigma^2(1 + y^2)}} \text{ and} \quad (\text{S37})$$

$$\frac{\partial \Theta^{\text{sin}}}{\partial x}(y, y) = -\frac{\partial \Theta^{\text{cos}}}{\partial x}(y, y) = \sigma^2 y e^{-2\sigma^2(1+y^2)}. \quad (\text{S38})$$

However, if the value of σ is too large, $\Theta(x, y)$ and, therefore, the dynamical system f_∞^* qualitatively change (Fig. S12). For $\phi = \text{sin}, \text{cos}$, the trained maps become the Kronecker-delta-like discontinuous functions that behave as constant functions except at \mathcal{D} , meaning that perturbations of x_0 from \mathcal{D} lead to their different attractors for a large σ :

$$\lim_{\sigma \rightarrow \infty} \Theta^{\text{sin}}(x, y) = \lim_{\sigma \rightarrow \infty} \Theta^{\text{cos}}(x, y) = \frac{1}{2} \mathbf{1}_y(x), \text{ where } \mathbf{1}_y(x) \equiv \begin{cases} 1 & (x = y) \\ 0 & (\text{otherwise}) \end{cases}, \quad (\text{S39})$$

$$\lim_{\sigma \rightarrow \infty} f_\infty^{*,\text{sin}}(x) = \lim_{\sigma \rightarrow \infty} f_\infty^{*,\text{cos}}(x) = \frac{1}{2} [\mathbf{1}_a(x) \ \mathbf{1}_b(x) \ \mathbf{1}_c(x)] (2I) \begin{bmatrix} b \\ c \\ a \end{bmatrix} = b\mathbf{1}_a(x) + c\mathbf{1}_b(x) + a\mathbf{1}_c(x), \text{ and} \quad (\text{S40})$$

$$\lim_{\sigma \rightarrow \infty} f_\infty^{*,\text{sin}}(\mathcal{X}) = \lim_{\sigma \rightarrow \infty} f_\infty^{*,\text{cos}}(\mathcal{X}) = \mathcal{Y}, \quad \lim_{\sigma \rightarrow \infty} f_\infty^{*,\text{sin}}(x) = \lim_{\sigma \rightarrow \infty} f_\infty^{*,\text{cos}}(x) = 0 \quad (x \notin \{a, b, c\}). \quad (\text{S41})$$

For $\phi = \text{erf}$, the trained map becomes the piecewise-monotonic and piecewise-smooth function, with \mathcal{D} being its singular points:

$$\lim_{\sigma \rightarrow \infty} \Theta^{\text{erf}}(x, y) = \frac{2}{\pi} \arcsin \frac{1 + xy}{\sqrt{(1 + x^2)(1 + y^2)}} \text{ and} \quad (\text{S42})$$

$$\frac{\partial}{\partial x} \lim_{\sigma \rightarrow \infty} \Theta^{\text{erf}}(x, y) = \frac{-2}{\pi(1 + x^2)} \cdot \frac{x - y}{|x - y|} = \begin{cases} \frac{2}{\pi} \cdot \frac{1}{1+x^2} & (x < y) \\ -\frac{2}{\pi} \cdot \frac{1}{1+x^2} & (x > y) \end{cases}, \quad (\text{S43})$$

enabling the candidates of robust chaos [14, 15] to appear (Fig. S12(b)). In particular, NTK for $\phi = \text{erf}$ is equivalent to that for binary activation ($\phi = \text{sgn}$) [16] in the limit $\sigma \rightarrow \infty$:

$$\Theta^{\text{sgn}}(x, y) = \frac{2}{\pi} \arcsin \frac{1 + xy}{\sqrt{(1 + x^2)(1 + y^2)}} = \lim_{\sigma \rightarrow \infty} \Theta^{\text{erf}}(x, y). \quad (\text{S44})$$

Although f_N^* for $\phi = \text{sgn}$ is beyond the scope of Sharkovsky's theorem (Theorem 1) and Li-Yorke's theorem (Theorem 2), it asymptotically approaches a continuous map f_∞^* , exhibiting multiple stable periodic orbits for a large N (Fig. S13).

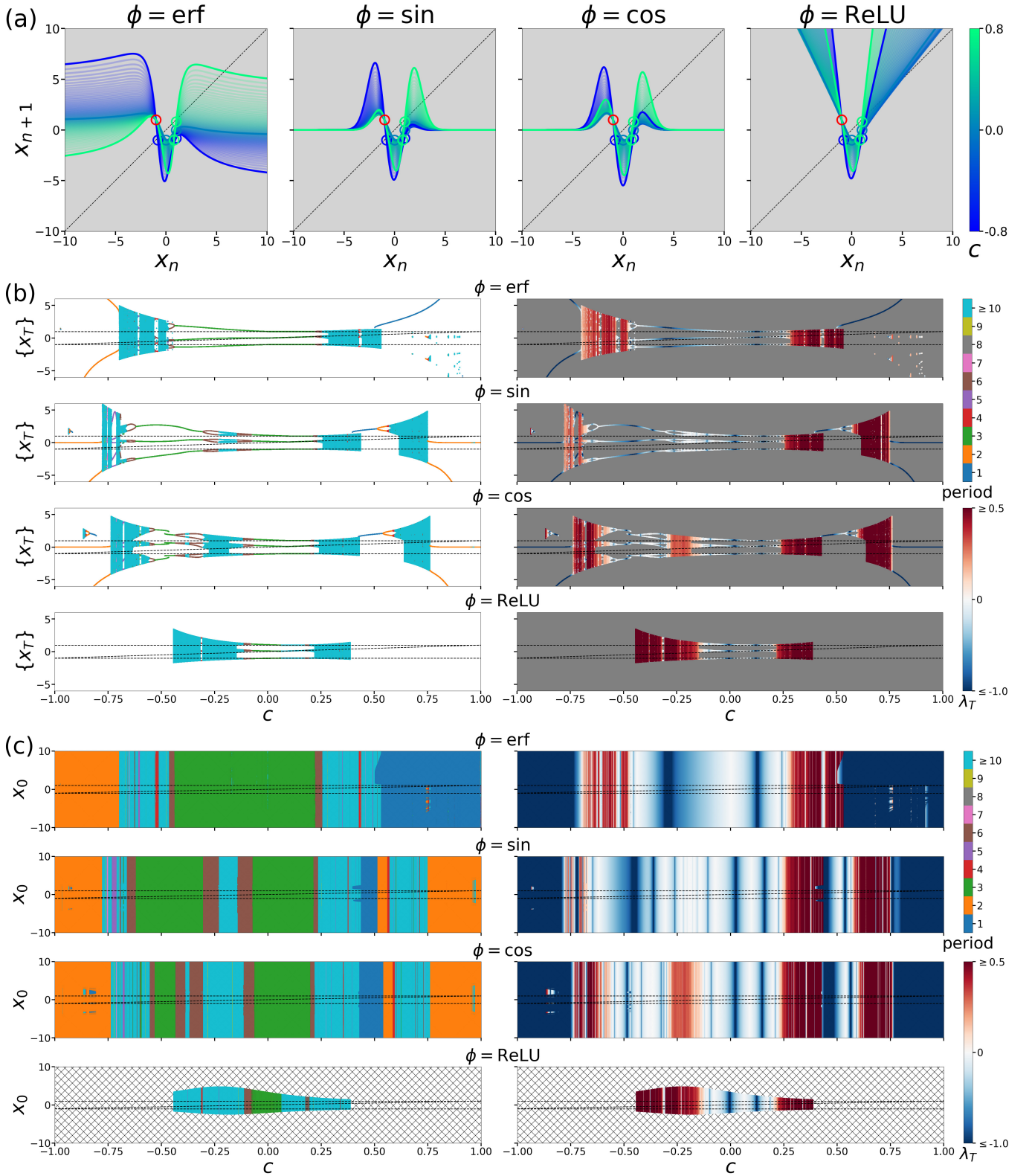


FIG. S6: One-dimensional bifurcation diagrams of the characteristic attractors of the dynamical system f_∞^* with respect to c , with $a = -1$, $b = 1$, $\sigma = 1.0$, and $T = 10^5$. (a) Change in the map f_∞^* in $-0.8 \leq c \leq 0.8$. (b) Change in the characteristic attractors calculated with $-10 \leq x_0 \leq 10$. (c) Change in the basin of attraction. The black-hatched area indicates the region (c, x_0) , where the trajectory heads toward infinity.

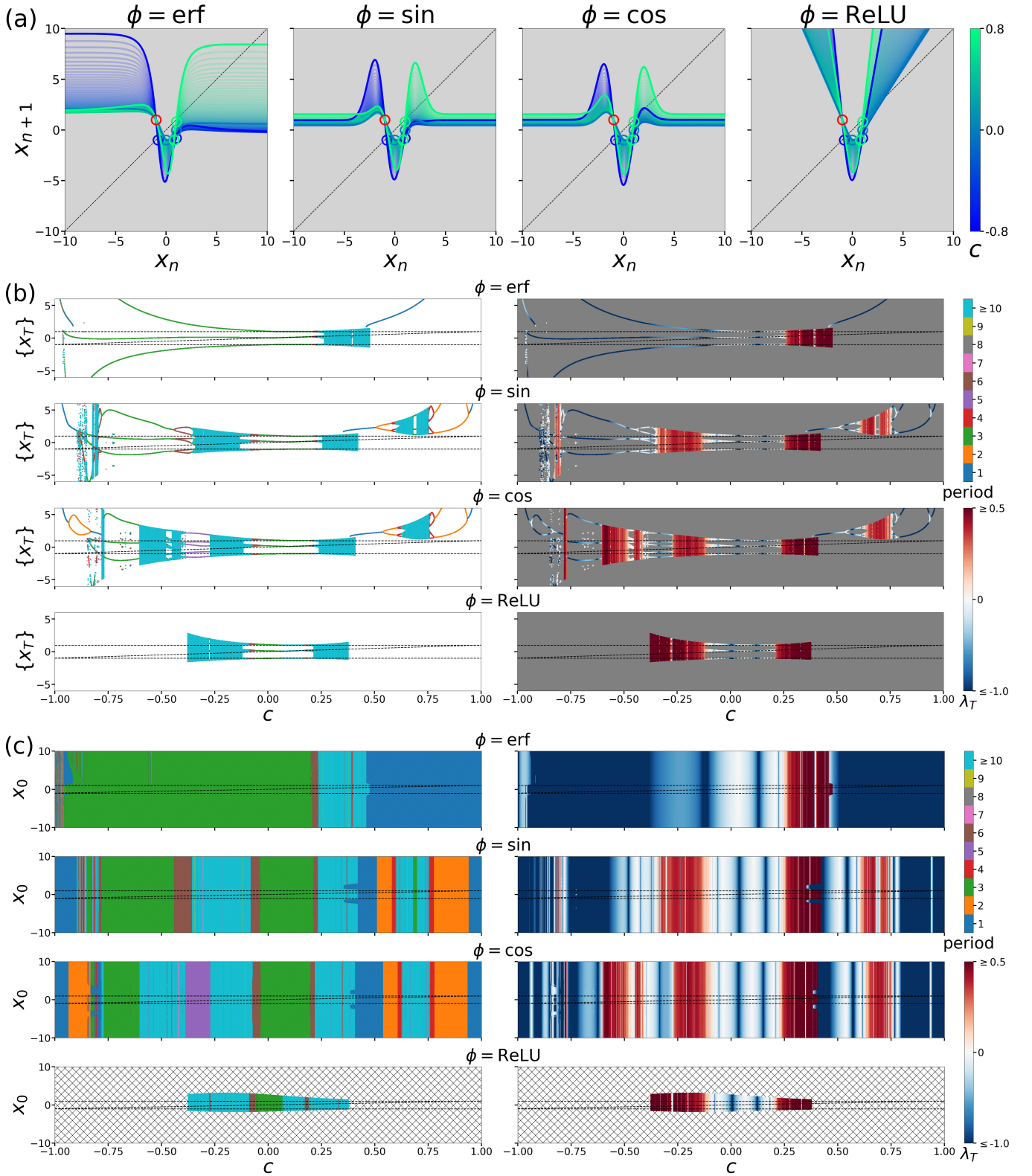


FIG. S7: One-dimensional bifurcation diagrams of the characteristic attractors of the dynamical system $f_\infty^{*,\text{bias}}$ with respect to c , with $a = -1$, $b = 1$, $\sigma = 1.0$, and $T = 10^5$. (a) Change in the map $f_\infty^{*,\text{bias}}$ in $-0.8 \leq c \leq 0.8$. (b) Change in the characteristic attractors calculated with $-10 \leq x_0 \leq 10$. (c) Change in the basin of attraction. The black-hatched area indicates the region (c, x_0) , where the trajectory heads toward infinity.

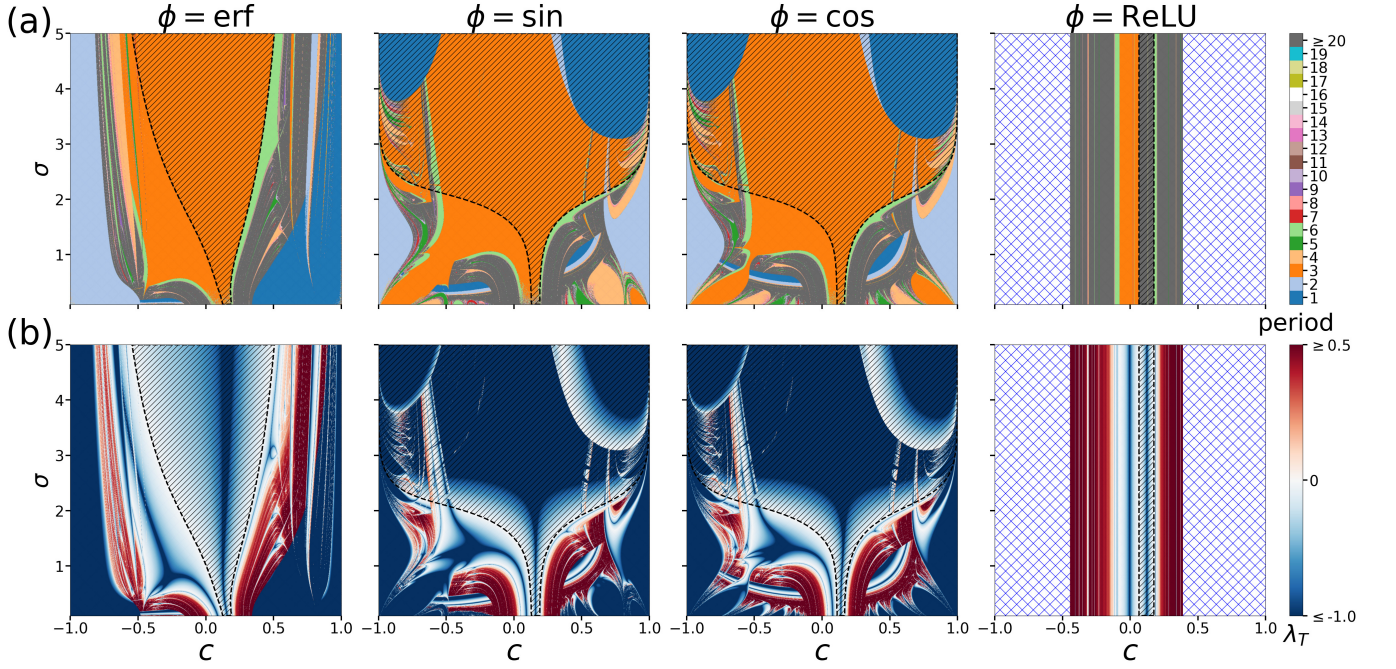


FIG. S8: Two-dimensional slices of the bifurcation of characteristic attractors of the dynamical system f_{∞}^* with respect to c and σ , with $a = -1$, $b = 1$, $x_0 = 0$, and $T = 10^4$. (a) Period of attractors. (b) Lyapunov exponents. The black-hatched areas indicate the regions in which $\left| \frac{df_{\infty}^*}{dx}(a) \frac{df_{\infty}^*}{dx}(b) \frac{df_{\infty}^*}{dx}(c) \right| < 1$ holds. They correspond to the regions of $\mathcal{D} = \{a, b, c\}$ being locally stable, implying that for $\phi = \text{erf}, \text{sin}, \text{cos}$, increasing σ tends to stabilize \mathcal{D} . The blue-hatched area indicates the region (c, σ) , where the trajectory starting from $x_0 = 0$ heads toward infinity.

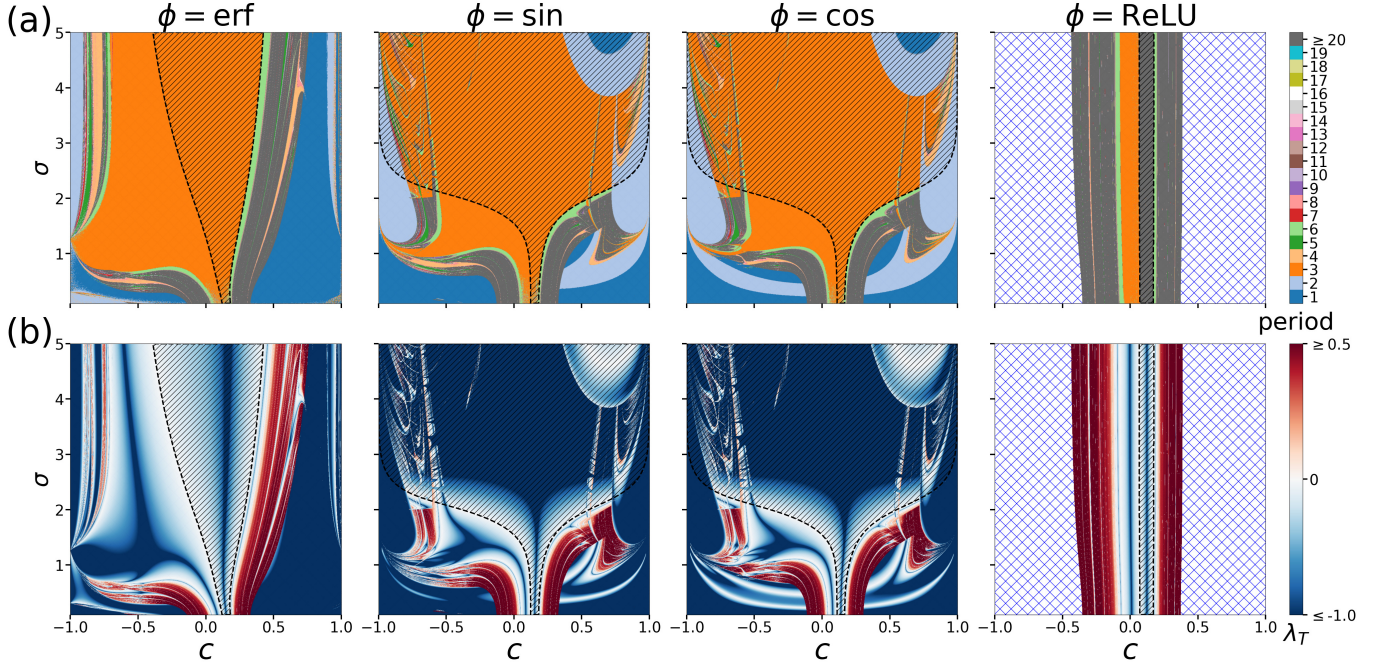


FIG. S9: Two-dimensional slices of the bifurcation of characteristic attractors of the dynamical system $f_{\infty}^{*,\text{bias}}$ with respect to c and σ , with $a = -1$, $b = 1$, $x_0 = 0$, and $T = 10^4$. (a) Period of attractors. (b) Lyapunov exponents. The black-hatched areas indicate the regions in which $\left| \frac{df_{\infty}^{*,\text{bias}}}{dx}(a) \frac{df_{\infty}^{*,\text{bias}}}{dx}(b) \frac{df_{\infty}^{*,\text{bias}}}{dx}(c) \right| < 1$ holds. The blue-hatched area indicates the region (c, σ) , where the trajectory starting from $x_0 = 0$ heads toward infinity.

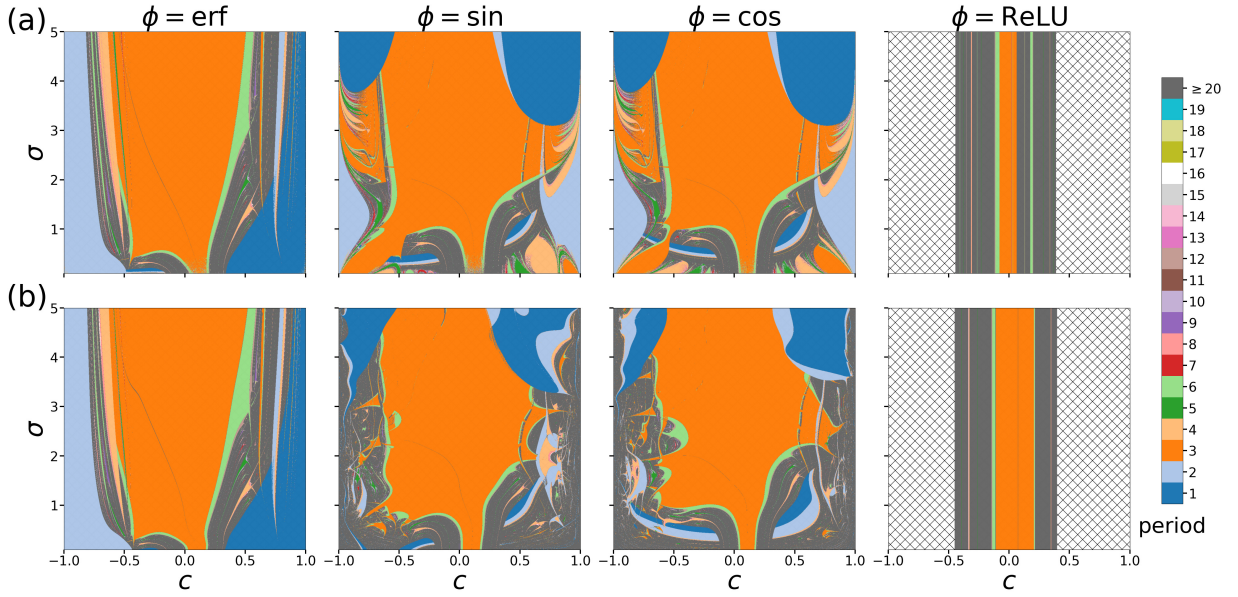


FIG. S10: Comparison of the bifurcations of characteristic attractors of (a) f_∞^* and (b) f_{1000}^* with respect to c and σ , with $a = -1$, $b = 1$, $x_0 = 0$, and $T = 10^4$. The black-hatched area indicates the region (c, σ) , where the trajectory starting from $x_0 = 0$ heads toward infinity.

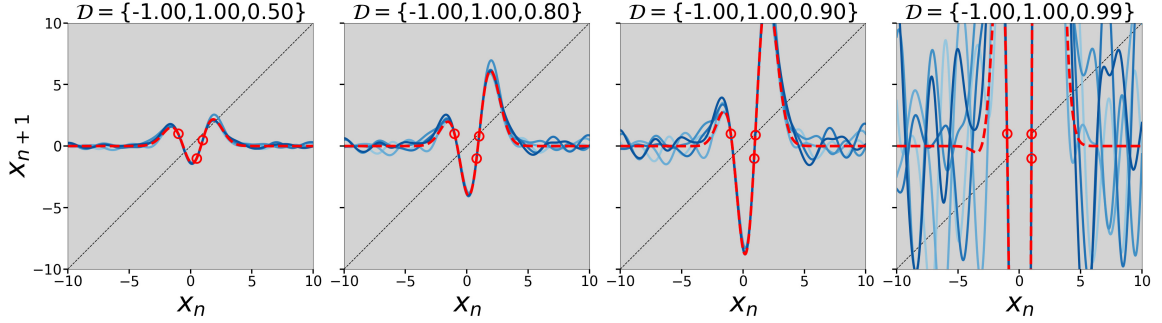


FIG. S11: Trained maps f_{1000}^* and f_∞^* for $\phi = \sin$ with $a = -1$, $b = 1$, and $\sigma = 1.0$. The red circles and the red dotted lines show target period three and f_∞^* , respectively. The blue solid lines indicate five different realizations of f_{1000}^* , illustrating that the wavy deviations of f_N^* from f_∞^* increase as c approaches a or b .

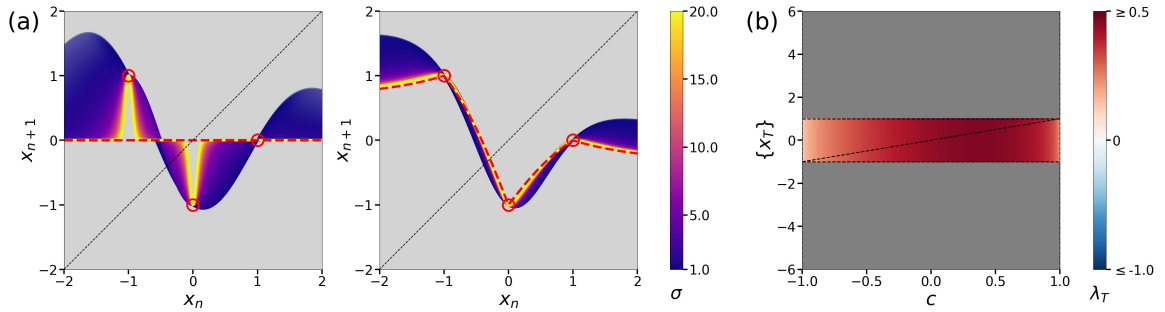


FIG. S12: Dynamical systems f_∞^* in the limit $\sigma \rightarrow \infty$, with $a = -1$ and $b = 1$. (a) Change in the map f_∞^* for $\phi = \sin$ (left) and erf (right) with respect to σ , with $c = 0$ fixed. The red circles and the red dotted lines show the target period three and $\lim_{\sigma \rightarrow \infty} f_\infty^*$, respectively. (b) Bifurcation diagram of the characteristic attractors of $\lim_{\sigma \rightarrow \infty} f_\infty^*$ for $\phi = \text{erf}$ with respect to c calculated with $-10 \leq x_0 \leq 10$. In this limit, f_∞^* for $\phi = \text{erf}$ becomes piecewise-monotonic and piecewise-smooth, with target period three being its singular points. In this setting, f_∞^* exhibits the candidate of robust chaos.

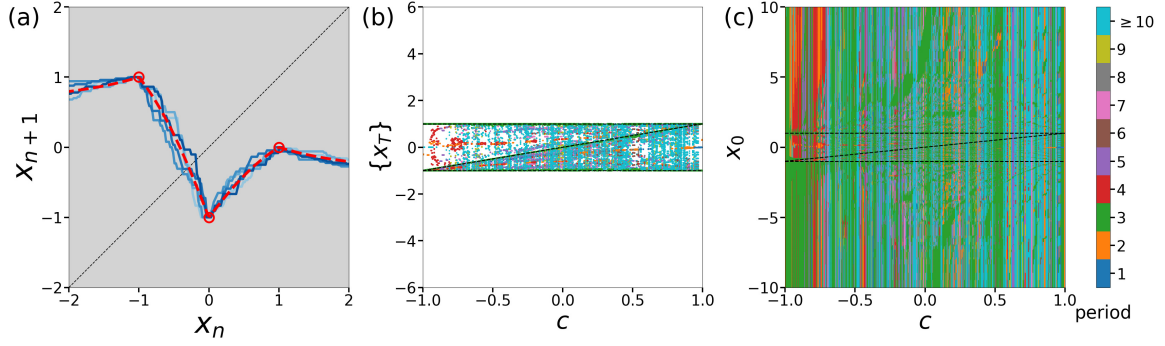


FIG. S13: Finite-size effects of the learning machine for $\phi = \text{sgn}$, with $a = -1$ and $b = 1$. (a) Trained maps f_N^* and f_∞^* , with $c = 0$ and $N = 100$. The red circles and the red dotted line show target period three and f_∞^* , respectively. The blue solid lines indicate five different realizations of f_N^* . (b) Bifurcation diagram of the attractors and (c) change in the basin of attraction calculated with $-10 \leq x_0 \leq 10$, $N = 10^3$, $T = 10^3$, and fixed realizations of the input layer. The complex structure in (c) corresponds to the discontinuity of f_N^* , and the trained network with $\phi = \text{sgn}$ qualitatively changes in its thermodynamic limit.

V. LEARNING PERIOD $n = 1, 2, 3, \dots$

In this section, we consider learning period $n = 1, 2, 3, \dots$ to investigate how the target period n affects the dynamical systems properties of learning machines. Assuming that $\mathcal{D} = \{a_1, \dots, a_{n-1}, a_n\}$, we obtain the following formula for the trained network output in learning period n :

$$f_\infty^*(x) = [\Theta(x, a_1) \cdots \Theta(x, a_{n-1}) \Theta(x, a_n)] \begin{bmatrix} \Theta(a_1, a_1) & \cdots & \Theta(a_1, a_{n-1}) & \Theta(a_1, a_n) \\ \vdots & \ddots & \vdots & \vdots \\ \Theta(a_{n-1}, a_1) & \cdots & \Theta(a_{n-1}, a_{n-1}) & \Theta(a_{n-1}, a_n) \\ \Theta(a_n, a_1) & \cdots & \Theta(a_n, a_{n-1}) & \Theta(a_n, a_n) \end{bmatrix}^{-1} \begin{bmatrix} a_2 \\ \vdots \\ a_n \\ a_1 \end{bmatrix}. \quad (\text{S45})$$

Fig. S14 shows examples of a trained map f_∞^* for $\phi = \text{erf}, \text{sin}, \text{cos}, \text{ReLU}$ in learning period $n = 1, 2, 3, 4, 5$. As n increases, the number of types of the target periodic orbit $(n-1)!$ explodes, making the shape of the trained map more complex.

To investigate how n affects the acquired periods, we analyzed the periodic points of period $p = 1, 2, \dots, 10$ in the map f_∞^* with a randomly drawn \mathcal{D} from the interval $[-10.0, 10.0]$ ($\mathcal{D} = \{-1, 1, c\}$ for Fig. 2(a) and $\mathcal{D} = \{-1, 1, 0\}$ for Fig. 3(b) in the main text) by solving the following nonlinear equation:

$$(f_\infty^*)^p(x_p) - x_p = 0, \quad (\text{S46})$$

using MATLAB `fsolve` command (Fig. S15). We uniformly chose 10^3 initial points from the interval $[-100.0, 100.0]$ ($[-10.0, 10.0]$ for Figs. 2(a) and 3(b) in the main text) to numerically solve Eq. (S46). To count the number of periodic orbits of period p , we used the absolute tolerance 10^{-2} to exclude the points belonging to the same periodic point, periodic orbit, and the periodic point of period $p' < p$ from the numerical solutions of Eq. (S46). We calculated the stability of the detected periodic orbit by computing $\lambda_p \equiv \ln \left| \frac{d}{dx} (f_\infty^*)^p(x_p) \right|$; we considered the periodic orbits of $\lambda_p < 0$ stable, and those of $\lambda_p > 0$, unstable. We note that the average distribution of periodic orbits of f_∞^* is invariant against the realizations of the random weights; however, it is affected by the tolerance 10^{-2} and the choice of the initial points in numerical calculations.

Fig. S15 indicates that regardless of the choice of ϕ , the number of unstable periods tends to increase dramatically after $n = 3$. This phenomenon may correspond to the fact that there always exists an appropriate ordering of period $n \geq 3$ that induces all periods (a Stefan sequence [17] of length 3), as discussed in Sec. 8 in Ref. [17]. Meanwhile, learning period two leads to non-trivial phenomena, depending on the choice of $\mathcal{D} = \{a, b\}$ and ϕ . For $\phi = \text{ReLU}$, f_∞^* becomes similar to $f(x) = -x + \alpha$ ($\alpha \in \mathbb{R}$) for some choices of \mathcal{D} , resulting in a large amount of period-2 orbits (see also Fig. S14). For $\phi = \text{sin}, \text{cos}$, some choices of \mathcal{D} provide a large number of unstable periods in f_∞^* , thereby creating high-order periodic orbits, chaos, and multiple attractors in the bifurcation of characteristic attractors (Fig. S16).

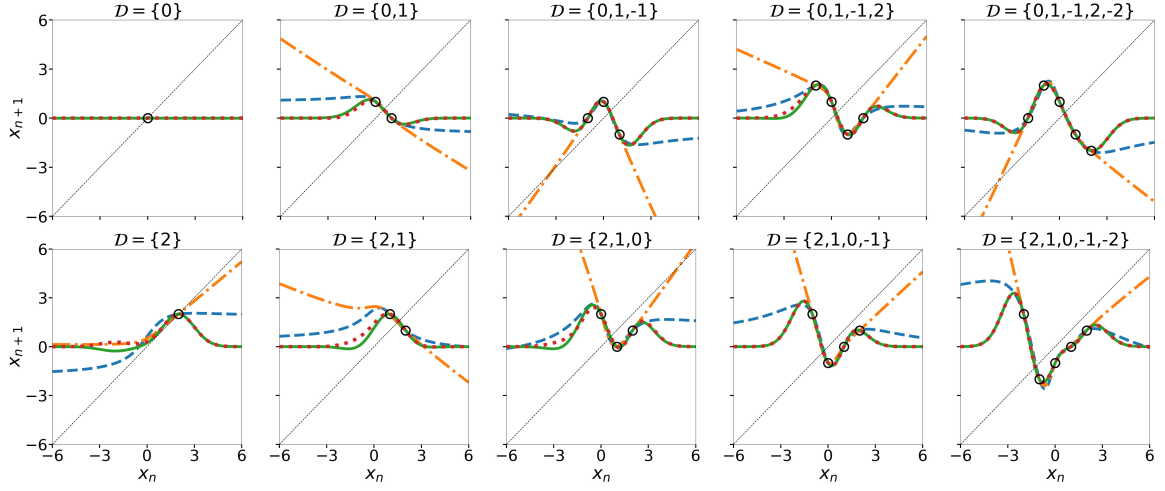


FIG. S14: Trained maps f_∞^* in learning period $n = 1, 2, 3, 4, 5$, with $\sigma = 1.0$ for $\phi = \text{erf}$ (blue line), \sin (green line), \cos (red line), and ReLU (orange line). Even in learning period $n = 1, 2$ (the two leftmost columns), where there is only one type of \mathcal{D} , f_∞^* depends on the value of the target data. Increasing n explodes the number of types of \mathcal{D} , resulting in the strong dependence of f_∞^* on the ordering of periodic points in \mathcal{D} , as can be seen in the case of learning period $n = 5$ (the rightmost column).

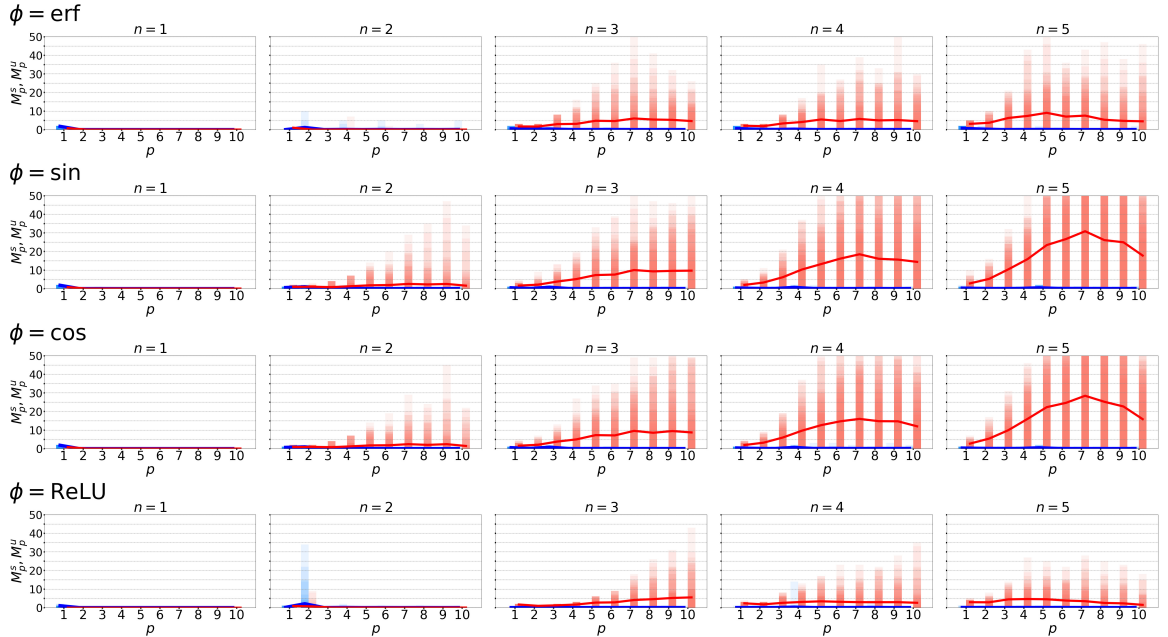


FIG. S15: Distribution of the acquired periods in learning period n , with $\sigma = 1.0$. Histograms for 100 different realizations of target data \mathcal{D} are overlaid for each n . The blue and red bins indicate the number of periodic orbits of period p with $\lambda_p < 0$ (stable, M_p^s) and $\lambda_p > 0$ (unstable, M_p^u), respectively. The solid lines show the average distributions of the acquired periods in learning period n . Periodic orbits of $\lambda_p = 0$ were not detected in this setting.

Note that in learning period two, f_∞^* is invariant under the swapping of a and b :

$$\begin{aligned}
 f_\infty^*(x)|_{\mathcal{D}=\{a,b\}} &= \frac{1}{\Theta(a,a)\Theta(b,b) - \Theta(a,b)^2} \begin{bmatrix} \Theta(x,a) & \Theta(x,b) \end{bmatrix} \begin{bmatrix} \Theta(b,b) & -\Theta(a,b) \\ -\Theta(b,a) & \Theta(a,a) \end{bmatrix} \begin{bmatrix} b \\ a \end{bmatrix} \\
 &= \frac{1}{\Theta(a,a)\Theta(b,b) - \Theta(a,b)^2} \begin{bmatrix} \Theta(x,b) & \Theta(x,a) \end{bmatrix} \begin{bmatrix} \Theta(a,a) & -\Theta(b,a) \\ -\Theta(a,b) & \Theta(b,b) \end{bmatrix} \begin{bmatrix} a \\ b \end{bmatrix} = f_\infty^*(x)|_{\mathcal{D}=\{b,a\}}.
 \end{aligned} \tag{S47}$$

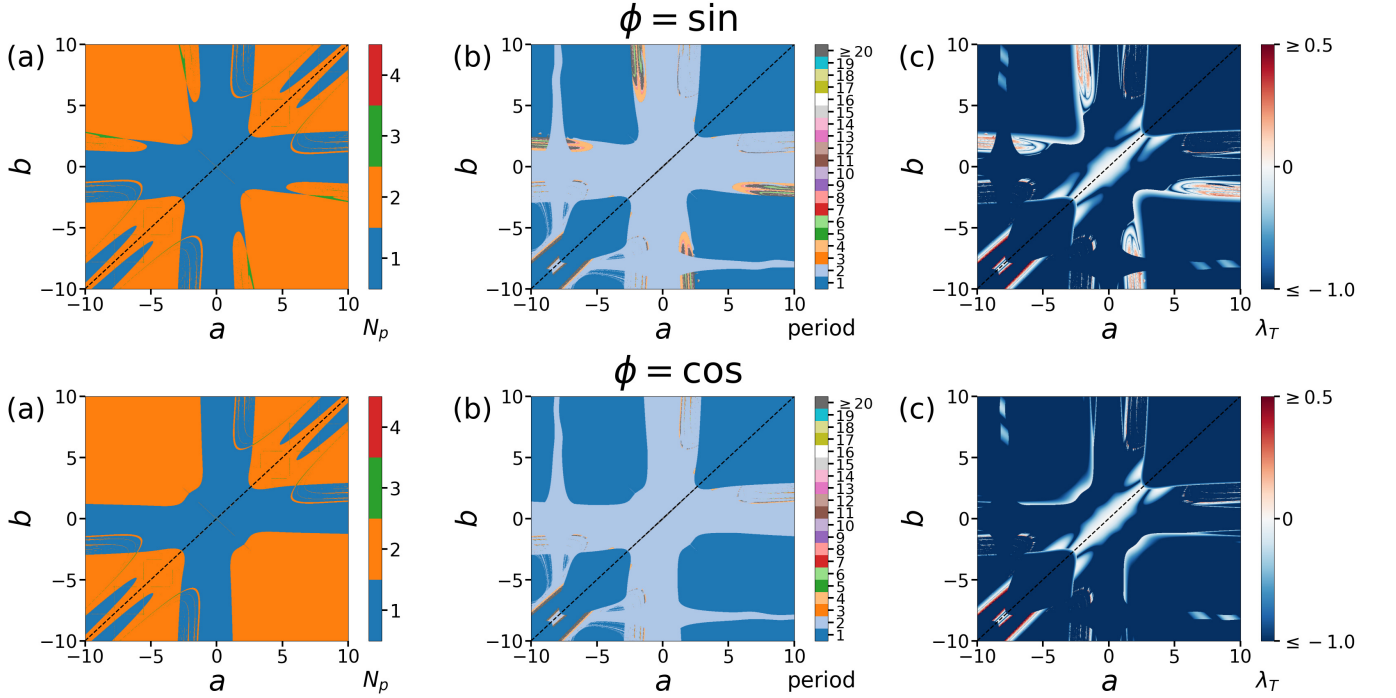


FIG. S16: Two-dimensional slices of the bifurcation of characteristic attractors of the dynamical system f_∞^* with respect to a and b , with $\sigma = 1.0$ and $T = 10^4$. (a) Number of kinds of periods of attractors N_p calculated with 100 equidistant initial states in $-10 \leq x_0 \leq 10$. f_∞^* has roughly N_p attractors. (b) Period of attractors and (c) Lyapunov exponents calculated with $x_0 = -8$. The dotted lines represent $a = b$, and the bifurcation structure is symmetric about $a = b$ (Eq. (S47)).

VI. EXTERNALIZATION OF THE LATENTLY EXISTING UNSTABLE PERIODS

In this section, we discuss the externalization $\sigma_{\text{fb}}, f_N^*$ of the latently existing unstable periods induced by learning period $n = 1, 2, 3$. Fig. S17 shows several examples of $\phi = \text{erf}, \sin, \cos, \text{ReLU}$ in learning period $n = 3$, with $N = \infty$. Although the way of externalization depends on \mathcal{D} and the network settings, we found that some universal externalizations appear when $\mathcal{D} = \{0\}, \{a, -a\}, \{a, -a, 0\}$ (“symmetric learning period $n = 1, 2, 3$ ”; Figs. S18–S20). Hereafter, we make the following assumptions (we discuss what kinds of networks satisfy these assumptions at the end of this section):

1. For a given ϕ and distributions of W^{in} and b^{in} , the kernel $\hat{\Theta}(x, y)$ (Eq. (4)) converges to a deterministic limiting kernel $\Theta(x, y)$.
2. The Gram matrix Θ (Eq. (3)) has full rank.
3. $\Theta(x, y) = \Theta(-x, -y)$ for any $x, y \in \mathbb{R}$.
4. $\Theta(x, y)$ is twice differentiable at $x = y = 0$.
5. $\Theta(0, 0) > 0$ and $\frac{\partial^2 \Theta}{\partial x \partial y}(0, 0) > 0$.

Note that if W^{in} and b^{in} are drawn from Gaussian distributions, $\phi = \text{erf}, \sin, \cos$ satisfy these conditions. Let us begin with the trivial case: symmetric learning period $n = 1$, where the resulting map f_∞^* will be a zero function, as follows:

$$f_\infty^*(x)|_{\mathcal{D}=\{0\}} = \frac{\Theta(x, 0)}{\Theta(0, 0)} \cdot 0 = 0. \quad (\text{S48})$$

Thus, the externalization $\sigma_{\text{fb}}, f_\infty^*(x)|_{\mathcal{D}=\{0\}}$ is topologically conjugate to the universal “dynamical system” $\sigma_{\text{fb}}, \hat{g}_1(x) \equiv 0$, which has a fixed point $x = 0$ as its unique attractor.

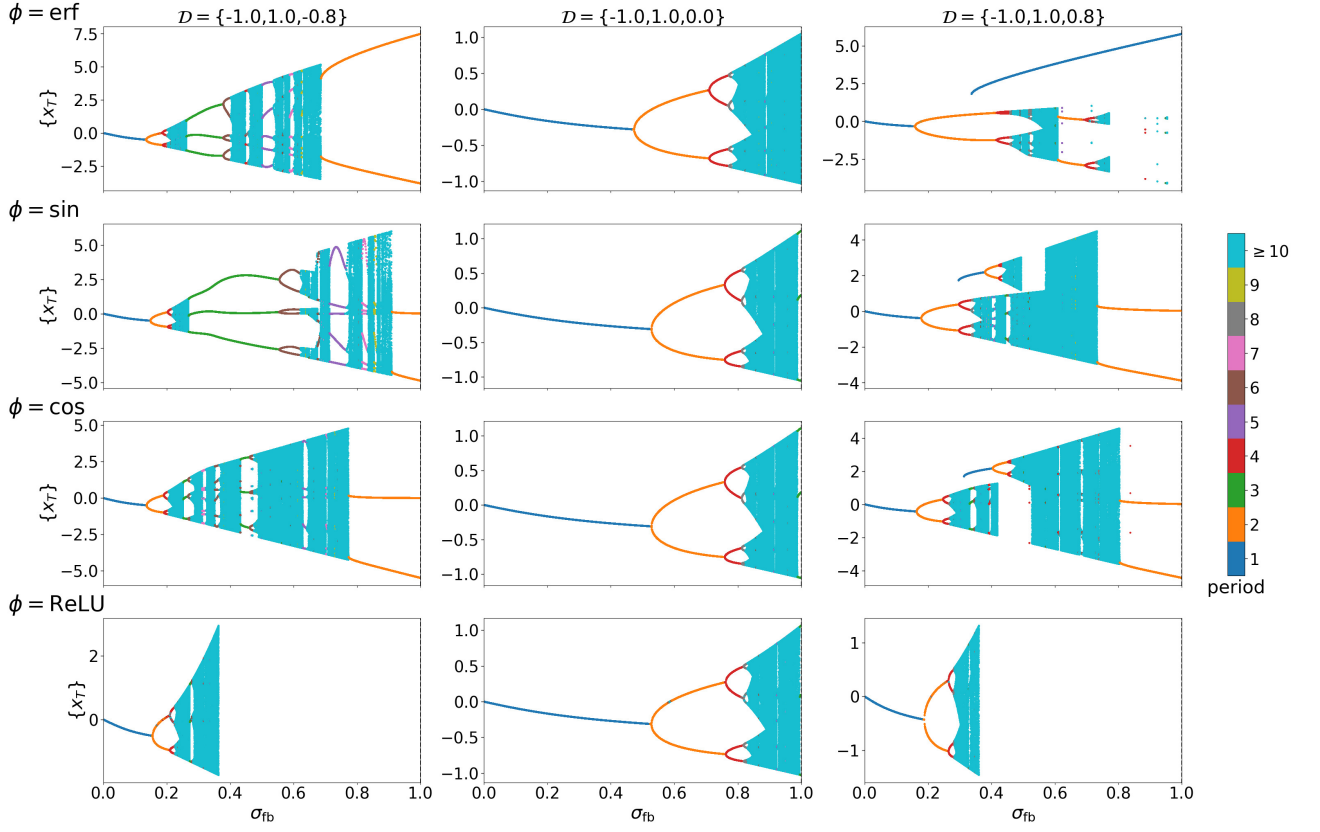


FIG. S17: Bifurcation diagrams of the trained neural networks $\sigma_{\text{fb}} f_{\infty}^*$ with respect to the feedback strength σ_{fb} , calculated with $\sigma = 1$, $-10 \leq x_0 \leq 10$, and $T = 10^5$.

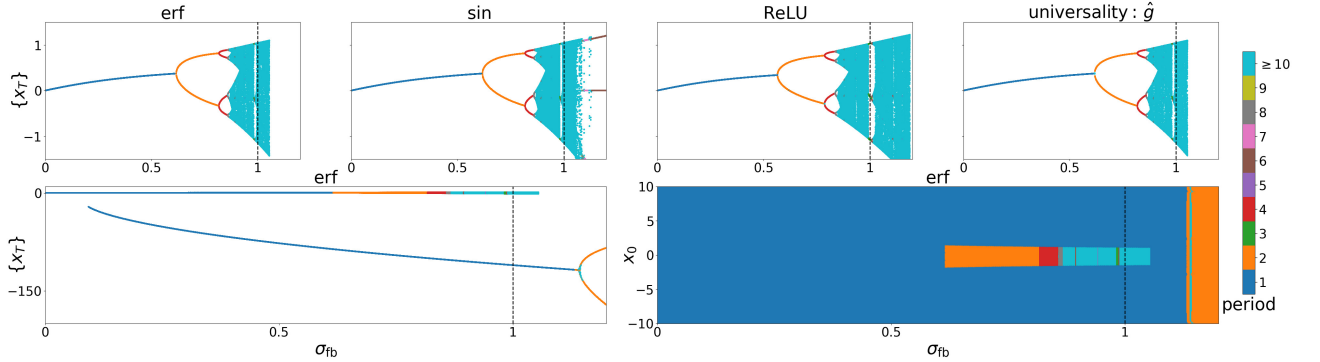


FIG. S18: Externalization $\frac{\sigma_{\text{fb}}}{a} f_{\infty}^*(ax)$ with $\sigma = 0.855$ and $\mathcal{D} = \{0.05, -0.05, 0\}$, calculated with $-10 \leq x_0 \leq 10$, $T = 10^4$, and $\varepsilon = 10^{-6}$. The top-right panel corresponds to the universal externalization, which is the bifurcation of $\sigma_{\text{fb}} \hat{g}(x)$ with respect to σ_{fb} . The externalization for $\phi = \text{ReLU}$ slightly differs from the universality \hat{g} . The bottom panels illustrate the coexistence of the controlled attractors and the characteristic attractors in the externalization $\sigma_{\text{fb}} f_{\infty}^*$ for $\phi = \text{erf}$. If ϕ is a bounded function, the attractor of $f_{\infty}^*(x)$ will switch to the characteristic attractor when \hat{g}_3 causes a boundary crisis [18] at $\sigma_{\text{fb}}(\mu)|_{\mu=4} = \frac{2}{25}(\sqrt{201} - 1) = 1.054\dots$

Next, applying $b = -a$ to Eq. (S47), f_{∞}^* in symmetric learning period $n = 2$ is given by the following equation:

$$f_{\infty}^*(x)|_{\mathcal{D}=\{a,-a\}} = -\frac{a}{\Theta(a,a) - \Theta(a,-a)} \{\Theta(x,a) - \Theta(x,-a)\}. \quad (\text{S49})$$

Eq. (S49) satisfies not only $f_{\infty}^*(\mathcal{X}) = \mathcal{Y}$ (target period two) but also $f_{\infty}^*(0) = 0$ (the fixed point). In addition, the

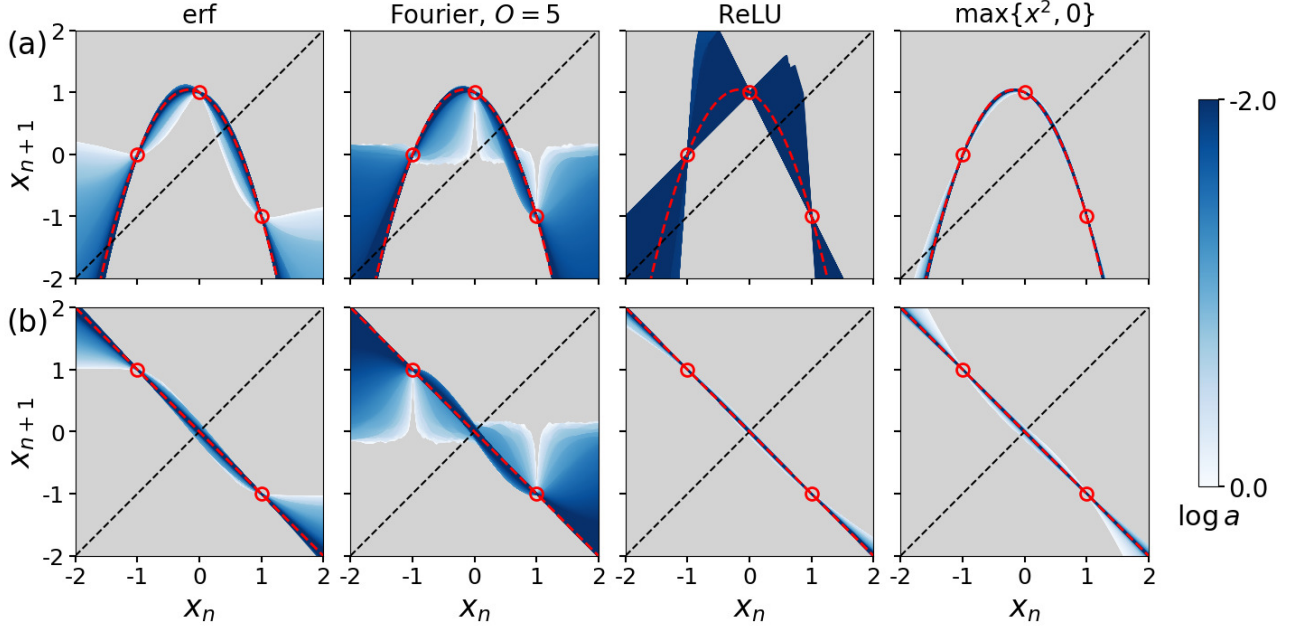


FIG. S19: Degeneration of the rescaled trained maps $\frac{1}{a}f_{1000}^*(ax)$ into the universal dynamical system $\hat{g}(x)$ in (a) $\mathcal{D} = \{a, -a, 0\}$ ($\hat{g}_3(x) = 1 - \frac{x}{2} - \frac{3x^2}{2}$) and (b) $\mathcal{D} = \{a, -a\}$ ($\hat{g}_2(x) = -x$). The scale of weights σ was randomly chosen from $[0.1, 10.0]$. For comparison, we used the random Fourier series $\frac{a_0}{2} + \sum_{k=1}^O [a_k \cos(kx) + b_k \sin(kx)]$ and the non-smooth $\max\{x^2, 0\}$ as the activation ϕ . The blue-colored areas indicate the maximum–minimum regions of f_{1000}^* for 100 different realizations. The red circles and the red dotted lines show \mathcal{D} and \hat{g} , respectively. The darkness of blue corresponds to a , describing that f_N^* , with certain activations and $N \gg 1$, degenerates into \hat{g} as a decreases.

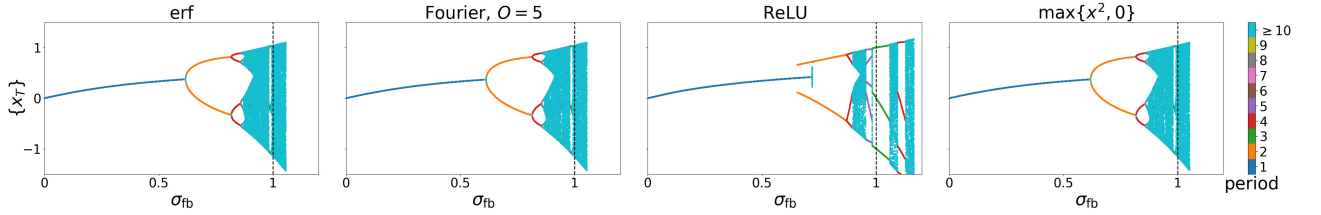


FIG. S20: Externalization $\frac{\sigma_{fb}}{a}f_{100}^*(ax)$ with $\sigma = 0.855$ and $\mathcal{D} = \{0.05, -0.05, 0\}$, calculated with $-10 \leq x_0 \leq 10$, $T = 10^3$, and $\varepsilon = 10^{-6}$. Although $N < \infty$, the externalizations, except for $\phi = \text{ReLU}$, are quite similar to the universality \hat{g} , which coincides with the degeneration of $f_N^*(x)$ in Fig. S19.

derivative of $f_\infty^*(x)$ at $x = 0$ is as follows:

$$\left. \frac{df_\infty^*}{dx}(0) \right|_{\mathcal{D}=\{a, -a\}} = -\frac{2a \frac{\partial \Theta}{\partial x}(0, a)}{\Theta(a, a) - \Theta(a, -a)} = -\frac{2 \frac{\partial^2 \Theta}{\partial x \partial y}(0, 0) + \mathcal{O}(a)}{2 \frac{\partial^2 \Theta}{\partial x \partial y}(0, 0) + \mathcal{O}(a)} \rightarrow -1 \quad (a \rightarrow 0), \quad (\text{S50})$$

where we Taylor-expand $\Theta(a, a)$, $\Theta(a, -a)$, and $\frac{\partial \Theta}{\partial x}(0, a)$ with respect to a :

$$\begin{aligned} \Theta(a, a) &= \Theta(0, 0) + a^2 \left\{ \frac{\partial^2 \Theta}{\partial x^2}(0, 0) + \frac{\partial^2 \Theta}{\partial x \partial y}(0, 0) \right\} + \mathcal{O}(a^3), \\ \Theta(a, -a) &= \Theta(0, 0) + a^2 \left\{ \frac{\partial^2 \Theta}{\partial x^2}(0, 0) - \frac{\partial^2 \Theta}{\partial x \partial y}(0, 0) \right\} + \mathcal{O}(a^3), \text{ and} \\ \frac{\partial \Theta}{\partial x}(0, a) &= a \frac{\partial^2 \Theta}{\partial x \partial y}(0, 0) + \mathcal{O}(a^2). \end{aligned} \quad (\text{S51})$$

For $a \ll 1$, its shape around $\mathcal{D} = \{a, -a\}$ is well described as a second-order polynomial function $\hat{g}_2(x)$. Imposing $\hat{g}_2(\mathcal{X}) = \mathcal{Y}$, $\hat{g}_2(0) = 0$, and $\frac{d\hat{g}_2}{dx}(0) = -1$, it is uniquely determined as $\hat{g}_2(x) = -x$. Thus, for a small a , period-2

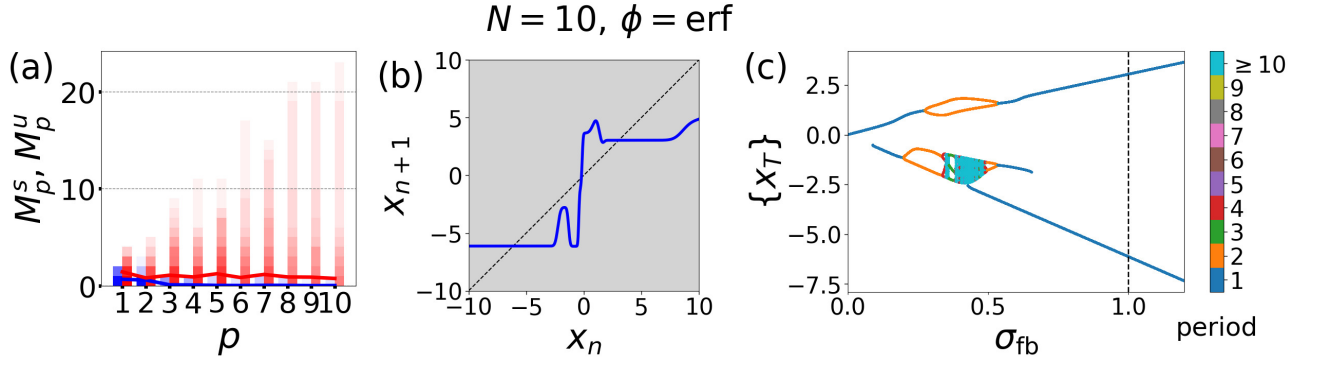


FIG. S21: Latently acquired periods in the random neural network f_N with the random network weights W^{in} and W^{out} generated from $\mathcal{N}(0, 5.0)$. (a) Distribution of periods. (b) Example of f_N . (c) Externalization $\sigma_{\text{fb}} f_N$, calculated with $-10 \leq x_0 \leq 10$ and $T = 10^3$. Histograms for 100 different realizations of the network weights W^{in} and W^{out} are overlaid. The blue and red bins indicate the number of stable (M_p^s) and unstable (M_p^u) periods p , respectively. The solid lines in the left panel show the average distributions of the acquired periods.

orbits of $\sigma_{\text{fb}} f_\infty^*(x)|_{\mathcal{D}=\{a, -a\}}$, acquired through learning period two ($\sigma_{\text{fb}} = 1$), will disappear in $0 \leq \sigma_{\text{fb}} < 1$, while the remaining fixed point $x = 0$ becomes its unique attractor around \mathcal{D} .

On the other hand, symmetric learning period $n = 3$ induces a universal dynamical system \hat{g}_3 that externalizes all types of periodic orbits in $0 \leq \sigma_{\text{fb}} < 1$. Applying $c = 0$ to both Eqs. (S32) and (S33), f_∞^* is given as follows:

$$f_\infty^*(x)|_{\mathcal{D}=\{a, -a, 0\}} = -\frac{a}{|\Theta|} [\Theta(x, a) \{\Theta(a, a)\Theta(0, 0) - \Theta(0, a)^2\} + \Theta(x, -a) \{\Theta(0, a)^2 - \Theta(a, -a)\Theta(0, 0)\} + \Theta(x, 0)\Theta(0, a) \{\Theta(a, -a) - \Theta(a, a)\}] + \frac{a}{|\Theta|} [\Theta(x, a)\Theta(0, a) \{\Theta(a, -a) - \Theta(a, a)\} + \Theta(x, -a)\Theta(0, a) \{\Theta(a, -a) - \Theta(a, a)\} + \Theta(x, 0) \{\Theta(a, a)^2 - \Theta(a, -a)^2\}] \text{ and} \quad (\text{S52})$$

$$|\Theta| = \Theta(0, 0) \{\Theta(a, a)^2 - \Theta(a, -a)^2\} + 2\Theta(0, a)^2 \{\Theta(a, -a) - \Theta(a, a)\}. \quad (\text{S53})$$

From the Taylor expansions of $\Theta(a, a)$, $\Theta(a, -a)$, and $\frac{\partial \Theta}{\partial x}(0, a)$, the derivative of $f_\infty^*(x)$ at $x = 0$ is given by

$$\left. \frac{df_\infty^*}{dx}(0) \right|_{\mathcal{D}=\{a, -a, 0\}} = -\frac{a \frac{\partial \Theta}{\partial x}(0, a)}{\Theta(a, a) - \Theta(a, -a)} = -\frac{\frac{\partial^2 \Theta}{\partial x \partial y}(0, 0) + \mathcal{O}(a)}{2 \frac{\partial^2 \Theta}{\partial x \partial y}(0, 0) + \mathcal{O}(a)} \rightarrow -\frac{1}{2} \quad (a \rightarrow 0). \quad (\text{14})$$

The third-order polynomial function g_3 that satisfies $g_3(\mathcal{X}) = \mathcal{Y}$ and $\frac{dg_3}{dx}(0) = -\frac{1}{2}$ is uniquely determined as follows:

$$g_3(x) = a \hat{g}_3\left(\frac{x}{a}\right) \text{ and } \hat{g}_3(x) \equiv 1 - \frac{x}{2} - \frac{3x^2}{2}, \quad (\text{S54})$$

which is topologically conjugate to the dynamical system $x_{n+1} = \hat{g}_3(x_n)$. As discussed in the main text, under $\mu > 2$, the externalization $x_{n+1} = \sigma_{\text{fb}} \hat{g}_3(x_n)$ is further topologically conjugate to the logistic map $y_{n+1} = \mu y_n(1 - y_n)$ in the following manner:

$$x_n = -\frac{2}{3} \left[\frac{\mu}{\sigma_{\text{fb}}(\mu)} \left(-y_n + \frac{1}{2} \right) + \frac{1}{4} \right], \quad (\text{16})$$

$$\sigma_{\text{fb}}(\mu) = \frac{4}{5} \sqrt{\frac{\mu}{2} \left(\frac{\mu}{2} - 1 \right) + \frac{1}{100} - \frac{2}{25}}. \quad (\text{17})$$

To derive Eqs. (16) and (17), we used the fact that for any polynomial of second degree like $f(x) = \alpha x^2 + \beta x + \gamma$, an affine linear mapping $h(x) = \alpha x + \frac{\beta}{2}$ satisfies

$$h(f(x)) = g(h(x)) \text{ for all } x \in \mathbb{R}, \quad (\text{S55})$$

where $g(x) = x^2 + c$ [19]. Here, the coefficients α , β and γ of $f(x)$ determine the constant term c of $g(x)$ as follows:

$$c = \alpha\gamma + \frac{\beta}{2} \left(1 - \frac{\beta}{2}\right). \quad (\text{S56})$$

Then, we can verify that Eq. (17) guarantees that the externalization $\sigma_{\text{fb}}\hat{g}_3(x_n)$ and the logistic map $\mu y_n(1 - y_n)$ share the same value of c (Eq. (S56)) for $\mu > 2$. The homeomorphism of this conjugacy (Eq. (16)) is, given by $h_{\text{ext}}^{-1} \circ h_{\text{log}}$, where $h_{\text{log}}(x) = \mu \left(-x + \frac{1}{2}\right)$ and $h_{\text{ext}}(x) = \sigma \left(-\frac{3}{2}x - \frac{1}{4}\right)$.

Controlling latently acquired periods with the externally tunable parameters \mathcal{D} and σ_{fb} emphasizes the necessity of LP3, since random neural networks without learning procedures sometimes acquire foldings, as in the logistic map [20], inducing an infinite number of the acquired periods (Fig. S21).

Finally, we discuss the plausible conditions of network settings for satisfying the aforementioned assumptions. If ϕ is a Lipschitz, continuous, and non-polynomial function, then the first and second assumptions will be satisfied according to Proposition 1 in Ref. [21] (a Lipschitz ϕ is required) and Theorem S1 (a non-polynomial and continuous ϕ is required), respectively. Then, if the distribution of W^{in} is symmetric at $W^{\text{in}} = 0$, the third assumption also holds, since

$$\Theta(-x, -y) = \mathbb{E}_{\omega, \beta} [\phi(-\omega x + \beta)\phi(-\omega y + \beta)] = \mathbb{E}_{-\omega, \beta} [\phi(\omega x + \beta)\phi(\omega y + \beta)] = \Theta(x, y). \quad (\text{S57})$$

For the fifth assumption, $\Theta(0, 0) > 0$ holds if the distribution of b^{in} has full support and ϕ is a non-zero function:

$$\Theta(0, 0) = \mathbb{E}_{\omega, \beta} [\phi(\beta)^2] > 0. \quad (\text{S58})$$

Allowing the interchange of limiting procedures and expectation, the fourth assumption will be satisfied if ϕ is twice differentiable and the distribution of W^{in} has the second moment:

$$\frac{\partial^2 \Theta}{\partial x^2}(0, 0) = \frac{\partial^2 \Theta}{\partial y^2}(0, 0) = \mathbb{E}_{\omega, \beta} [\omega^2 \phi^{(2)}(\beta)\phi(\beta)] = \mathbb{E}_{\omega} [\omega^2] \mathbb{E}_{\beta} [\phi^{(2)}(\beta)\phi(\beta)] \quad \text{and} \quad (\text{S59})$$

$$\frac{\partial^2 \Theta}{\partial x \partial y}(0, 0) = \mathbb{E}_{\omega, \beta} [\omega^2 \phi'(\beta)^2] = \mathbb{E}_{\omega} [\omega^2] \mathbb{E}_{\beta} [\phi'(\beta)^2], \quad (\text{S60})$$

implying that a non-constant differentiable ϕ will also satisfy the fifth assumption with a full-support distribution of b^{in} .

Therefore, we claim that the universalities \hat{g}_1 , \hat{g}_2 , and \hat{g}_3 appear, at least, in the networks for which the distributions of W^{in} and b^{in} are iid, full-support, and symmetric at the origin with the second moment, and the activation ϕ is non-polynomial and twice differentiable, with a bounded k -th derivative ($0 \leq k \leq 2$) (we used $\mathbb{E}[|\omega|] < \mathbb{E}[\omega^2 + 1]$ and $\mathbb{E}[\omega^2] < \infty$ to apply Lebesgue's dominated convergence theorem for the fourth and fifth assumptions). However, this condition seems too restrictive, as seen in the case of $\phi = \max\{x^2, 0\}$ in Figs. S19 and S20.

-
- [1] G.-B. Huang, Q.-Y. Zhu, and C.-K. Siew, Extreme learning machine: Theory and applications, *Neurocomputing* **70**, 489 (2006), neural Networks.
 - [2] Y. Itoh, Y. Tada, and M. Adachi, Reconstructing bifurcation diagrams with lyapunov exponents from only time-series data using an extreme learning machine, *Nonlinear Theory and Its Applications*, IEICE **8**, 2 (2017).
 - [3] Y. Itoh, S. Uenohara, M. Adachi, T. Morie, and K. Aihara, Reconstructing bifurcation diagrams only from time-series data generated by electronic circuits in discrete-time dynamical systems, *Chaos: An Interdisciplinary Journal of Nonlinear Science* **30**, 013128 (2020).
 - [4] C. Saunders, A. Gammerman, and V. Vovk, Ridge regression learning algorithm in dual variables, in *Proceedings of the 15th International Conference on Machine Learning*, ICML'98 (Morgan Kaufmann, San Francisco, CA, 1998) pp. 515–521.
 - [5] J. Suykens, Nonlinear modelling and support vector machines, in *IMTC 2001. Proceedings of the 18th IEEE Instrumentation and Measurement Technology Conference. Rediscovering Measurement in the Age of Informatics (Cat. No.01CH 37188)*, Vol. 1 (2001) pp. 287–294 vol.1.
 - [6] T. Liang and A. Rakhlin, Just interpolate: Kernel “ridgeless” regression can generalize, *The Annals of Statistics* **48**, 1329 (2020).
 - [7] T. Hastie, A. Montanari, S. Rosset, and R. J. Tibshirani, Surprises in high-dimensional ridgeless least squares interpolation, *The Annals of Statistics* **50**, 949 (2022).
 - [8] L. Carvalho, J. L. Costa, J. Mourão, and G. Oliveira, The positivity of the neural tangent kernel (2024), arXiv:2404.12928 [cs.LG].
 - [9] S. Tamura and M. Tateishi, Capabilities of a four-layered feedforward neural network: four layers versus three, *IEEE Transactions on Neural Networks* **8**, 251 (1997).

- [10] C. Williams, Computing with infinite networks, in *Advances in Neural Information Processing Systems*, Vol. 9, edited by M. Mozer, M. Jordan, and T. Petsche (MIT Press, 1996).
- [11] Y. Cho and L. Saul, Kernel methods for deep learning, in *Advances in Neural Information Processing Systems*, Vol. 22, edited by Y. Bengio, D. Schuurmans, J. Lafferty, C. Williams, and A. Culotta (Curran Associates, Inc., 2009).
- [12] W. De Melo and S. Van Strien, *One-Dimensional Dynamics* (Springer, Berlin, 1993).
- [13] S. v. Strien, T. Bedford, and H. Swift, Smooth dynamics on the interval (with an emphasis on quadratic-like maps), in *New Directions in Dynamical Systems*, London Mathematical Society Lecture Note Series (Cambridge University Press, 1988) p. 57–119.
- [14] S. Banerjee, J. A. Yorke, and C. Grebogi, Robust chaos, *Phys. Rev. Lett.* **80**, 3049 (1998).
- [15] S. Banerjee, M. Karthik, G. Yuan, and J. Yorke, Bifurcations in one-dimensional piecewise smooth maps-theory and applications in switching circuits, *IEEE Transactions on Circuits and Systems I: Fundamental Theory and Applications* **47**, 389 (2000).
- [16] J. Dong, E. Börve, M. Rafayelyan, and M. Unser, Asymptotic stability in reservoir computing, in *2022 International Joint Conference on Neural Networks (IJCNN)* (2022) pp. 01–08.
- [17] K. Burns and B. Hasselblatt, The sharkovsky theorem: A natural direct proof, *The American Mathematical Monthly* **118**, 229 (2011).
- [18] C. Grebogi, E. Ott, and J. A. Yorke, Crises, sudden changes in chaotic attractors, and transient chaos, *Physica D: Nonlinear Phenomena* **7**, 181 (1983).
- [19] H.-O. Peitgen, H. Jürgens, and D. Saupe, *Chaos and Fractals* (Springer New York, 2004).
- [20] S. Ishihara and K. Kaneko, Magic number 7 ± 2 in networks of threshold dynamics, *Phys. Rev. Lett.* **94**, 058102 (2005).
- [21] A. Jacot, F. Gabriel, and C. Hongler, Neural tangent kernel: Convergence and generalization in neural networks, in *Advances in Neural Information Processing Systems*, Vol. 31, edited by S. Bengio, H. Wallach, H. Larochelle, K. Grauman, N. Cesa-Bianchi, and R. Garnett (Curran Associates, Inc., 2018).